



Published in final edited form as:

Pharmacol Res. 2020 August ; 158: 104847. doi:10.1016/j.phrs.2020.104847.

Pseurotin A as a Novel Suppressor of Hormone Dependent Breast Cancer Progression and Recurrence by Inhibiting PCSK9 Secretion and Interaction with LDL Receptor

Khaldoun S. Abdelwahed¹, Abu Bakar Siddique¹, Mohamed M. Mohyeldin^{1,2}, Mohammed H. Qusa¹, Amira A. Goda^{1,3}, Sitanshu S. Singh¹, Nehad M. Ayoub⁴, Judy Ann King⁵, Seetharama D. Jois¹, Khalid A. El Sayed^{1,*}

¹School of Basic Pharmaceutical and Toxicological Sciences, College of Pharmacy, University of Louisiana at Monroe, 1800 Bienville Drive, Monroe, LA 71201, USA

²Department of Pharmacognosy, Faculty of Pharmacy, Alexandria University, Alexandria, 20521, Egypt

³Department of Food Contaminant and Toxicology, National Research Center, Cairo, 12622, Egypt

⁴Department of Clinical Pharmacy, Faculty of Pharmacy, Jordan University of Science and Technology, Irbid, 22110, Jordan

⁵Department of Pathology and Translational Pathobiology, LSU Health Shreveport, 1501 Kings Highway, Shreveport, LA 71103, USA

Abstract

Hypercholesterolemia has been documented to drive hormone-dependent breast cancer (BC) progression and resistance to hormonal therapy. Proprotein convertase subtilisin/kexin type-9 (PCSK9) regulates cholesterol metabolism through binding to LDL receptor (LDLR) and targeting the receptor for lysosomal degradation. Inhibition of PCSK9 is an established strategy to treat hypercholesterolemia. Pseurotin A (PS) is a unique spiro-heterocyclic γ -lactam alkaloid isolated from the fungus *Aspergillus fumigatus*. Preliminary studies indicated that PS lowered PCSK9 secretion in cultured HepG2 hepatocellular carcinoma cells, with an IC₅₀ value of 1.20 μ M. Docking studies suggested the ability of PS to bind at the PCSK9 narrow interface pocket that accommodates LDLR. Surface plasmon resonance (SPR) showed PS ability to inhibit the PCSK9-LDLR interaction at a concentration range of 10-150 μ M. PS showed *in vitro* dose-dependent reduction of PCSK9, along with increased LDLR levels in hormone-dependent BT-474 and T47D breast cancer (BC) cell lines. *In vivo*, daily oral 10 mg/kg PS suppressed the progression of the

*Correspondence: elsayed@ulm.edu; Tel.: +1-318-342-1725.

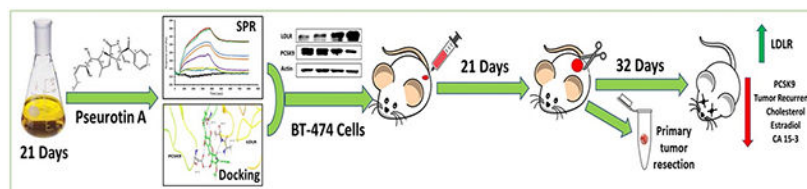
Publisher's Disclaimer: This is a PDF file of an unedited manuscript that has been accepted for publication. As a service to our customers we are providing this early version of the manuscript. The manuscript will undergo copyediting, typesetting, and review of the resulting proof before it is published in its final form. Please note that during the production process errors may be discovered which could affect the content, and all legal disclaimers that apply to the journal pertain.

Conflicts of Interest:

K. El Sayed is a Chief Scientific Officer in the Shreveport, Louisiana-based Oleolive without compensations. The other authors declare no conflict of interest.

hormone-dependent BT-474 BC cells in orthotopic nude mouse xenograft model. Immunohistochemistry (IHC) investigation of BT-474 breast tumor tissue proved the PS ability to reduce PCSK9 expression. PS also effectively suppressed BT-474 BC cells locoregional recurrence after primary tumor surgical excision. Western blot analysis showed decreased PCSK9 expression in liver tissues of PS-treated mice compared to vehicle-treated control group. PS treatment significantly reduced PCSK9 expression and normalized LDLR levels in collected primary and recurrent breast tumors at the study end. PS-treated mice showed reduced plasma cholesterol and 17β -estradiol levels. Inhibition of tumor recurrence was associated with significant reductions in plasma level of the human BC recurrence marker CA 15-3 in treated mice at the study end. Histopathological examination of various PS-treated mice organs indicated lack of metastatic tumor cells and any pathological changes. The results of this study provide the first evidence for the suppression of the hormone-dependent breast tumor progression and recurrence by targeting the PCSK9-LDLR axis. PS is a novel first-in-class PCSK9-targeting lead appropriate for the use to control hormone-dependent BC progression and recurrence.

Graphical abstract



Keywords

Breast cancer; CA 15-3; 17β -estradiol; Hypercholesterolemia; PCSK9; LDLR; Pseurotin A; Recurrence

1. Introduction

Breast cancer (BC) continues to be the most commonly diagnosed cancer in women worldwide and the second leading cause of women cancer death after lung cancer in the US [1]. The precise cause of BC is not yet fully understood. However, several risk factors may concurrently contribute to initiate and/or promote BC. Among these risk factors, there is a direct relationship between elevated low density lipoprotein-cholesterol (LDL-C) and very low density lipoprotein-cholesterol (VLDL-C) with BC development [2,3]. Early observation linking cholesterol with cancer was made in 1909 by noting the presence of crystals of a “fatty nature” in tumor sections [4]. Recent studies clearly delineate the contribution of cholesterol biosynthetic pathway to cancer pathogenesis, specifically in estrogen receptor-positive (ER^+) BC. The importance of cholesterol pathway in cancer was controversial until the Cancer Genome Atlas (TCGA) project profiled all mutated genes and proved the critical role the overexpressed cholesterol synthesis controlling genes play in cancer [5,6]. Tumor-induced hyperlipidemia initiates a feed-forward mechanism, which reprograms hepatic lipoprotein homeostasis to produce LDL-C, which supported tumor growth in multiple mouse models [7,8]. The oxysterols, cholesterol mammalian metabolites

25- and 27-hydroxycholesterol (25-/27HC) produced by CYP27A1 in liver cells and macrophages, are ER agonists and precursors for the biosynthesis of 17- β estradiol [5,6]. Therefore, there is a compelling evidence supporting the major role of hypercholesterolemia in hormone-dependent BC [8].

The proprotein convertases are Ca^{2+} -dependent serine proteases with homology to the endoproteases subtilisin (bacteria) and kexin (yeast) [9]. Circulating proprotein convertase subtilisin/kexin type-9 (PCSK9), produced in liver and other organs, bind to LDLR and promotes receptor-LDL complex trafficking to lysosomal compartment leading to degradation of complex and downregulation of total receptor as well as LDL levels [9]. The relationship between PCSK9 and LDL-C levels was discovered by defining PCSK9 mutation in patients with familial hypercholesterolemia [10]. Inhibiting PCSK9-mediated LDLR degradation with monoclonal antibodies is a valid strategy to lower circulating LDL-C evidenced by the FDA approved currently marketed humanized PCSK9 mAb drugs evolocumab (Repatha) and alirocumab (Praluent) [11]. The unique size and shape of the PCSK9 interface at which it interact with LDLR rendered the development of small-molecule protein-protein inhibitors (PPI) very challenging [12]. Hence, most current inhibitors of PCSK9-LDLR binding are protein or peptide domains based on chemical similarity to the LDLR EGF-A or EGF-AB domains [13,14], recombinant LDLR fragments [15], and mono- or polyclonal antibodies [16,17].

Pseurotin A (PS) was originally isolated from the fungal culture of *Pseudeurotium ovalis* (strain S2269/F) in 1976, but later reported in soil, endophytic, and marine *Aspergillus* and *Penicillium* species [18,19]. PS competitively inhibited the fungal chitin synthase [18], induced pheochromocytoma PC12 cells differentiation [19] and patented as apomorphine antagonist and bacteriostatic food preservative [20,21]. PS showed anti-inflammatory [22], and weak cytotoxic activity against mouse leukemia P388, human leukemia HL60, human lung carcinoma A-549 and human hepatic carcinoma BEL-7402 cell lines [23]. Recently, pseurotins showed anti-seizure activity discovered in zebrafish embryos and larvae model and validated in a mouse psychomotor seizure model and therefore were patented as anticonvulsant leads [24,25]. Pseurotins showed drug-likeness behavior in a comprehensive AMDT study [24]. PS also inhibited the formation and function of osteoclasts by suppressing RANKL-induced oxidative stress and downstream NFATc1 signaling and therefore was patented as a potential treatment and preventive for osteoporosis [26]. Pseurotins A and D recently proved to inhibit IgE production in B-cells by targeting the activation of STATs 3, 5, and 6 and therefore inhibited the B-cell proliferation and differentiation to plasma cells, *in vitro* [27]. Pseurotin D significantly inhibited the OVA-induced footpad swelling in a mouse model and therefore pseurotins are proposed as prospective anti-allergic leads [27]. In this study, PS is proposed as a novel dual PCSK9 secretion and PCSK9-LDLR interaction inhibitor with potent suppressive activities for hypocholesterolemia-induced ER⁺ BC progression and locoregional recurrence.

2. Materials and Methods

2.1. Chemicals, Reagents, and Antibodies

All chemicals were purchased from Sigma-Aldrich (St. Louis, MO, USA), unless otherwise stated. Organic solvents were purchased from VWR (Suwanee, GA, USA), dried by standard procedures, packaged under nitrogen in Sure/Seal bottles, and stored over 4 Å molecular sieves, unless otherwise indicated. Cell culture reagents were obtained from Life Sciences (Carlsbad, CA, USA). All antibodies were purchased from Cell Signaling Technology (Beverly, MA, USA) and used at a dilution of 1:1000, unless otherwise stated.

2.2. Fermentation and Isolation

The fungus *A. fumigatus* ATCC 26934 was cultured on yeast malt agar (41 g/L), after spore formation, spores were collected and prepared as a stock in sterile water-glycerin (10:1) and inoculated in SPS media (400 mL skimmed milk, 20 g potato dextrose broth, 20 g sucrose and the volume was completed to 1L with distilled water). Fermentation was conducted in 2 L Erlenmeyer flasks, each containing 700 mL SPS media and fermented on an orbital shaker (100 rpm) at room temperature. After 21 days, media was filtered, and the collected cell-free media was passed on Amberlite XAD-7 (Alfa Aesar, Tewksbury, MA, USA), washed with deionized water and finally eluted with acetone. The acetone eluate was evaporated under vacuum. The concentrated media was then extracted three times with ethyl acetate. The organic solvent was concentrated under reduced pressure to yield a crude extract, which was subjected to vacuum liquid chromatography on Si gel 60 (Natland International Corporation, 230–400 µm) using *n*-hexane-EtOAc, gradient elution starting with 100% *n*-hexane and ending with 100% EtOAc, to afford 8 fractions. Fractions containing PS were pooled, guided by TLC and ¹H NMR data, and further sub-fractionated over Si gel 60, using isocratic *n*-hexane-EtOAc-MeOH (v/v, 7:3:1.5) to afford PS with >99% purity based on q¹H NMR analysis, at a 10 mg/L fermentation yield.

2.3. Molecular Modeling

The predictive in-silico experiments were conducted using Schrödinger molecular modeling software package installed on an iMac 27-inch Z0PG workstation with a 3.5 GHz Quad-core Intel Core i7, Turbo Boost up to 3.9 GHz, processor and 16 GB RAM (Apple, Cupertino, CA, USA) to study the ability of PS to disrupt the PCSK9-LDLR interaction via binding at the PCSK9 active binding site.

2.3.1. Protein Structure Preparation—The PDB wild-type PCSK9 crystal structures (PDB codes: 4NE9, 4NMX, and 3GCW) and the mutant-type PCSK9 crystal structure PDB code: 3GCX were used. The Protein Preparation Wizard was implemented to prepare the active domain of each protein. The protein was reprocessed by assigning bond orders, adding hydrogens, creating disulfide bonds and optimizing H-bonding networks using PROPKA (Jensen Research Group, Denmark) [28]. Finally, energy minimization with RMSD value of 0.3 Å was applied using an Optimized Potentials for Liquid Simulation (OPLS_2005, Schrödinger, New York, USA) force field.

2.3.2. Ligand Structure Preparation—The chemical structure of PS was sketched on the Maestro 9.3 panel interface (Maestro, version 9.3, 2012, Schrödinger, USA). The Lig Prep 2.3 module (Lig Prep, version 2.3, 2012, Schrödinger, USA) was implemented to generate the 3D structure and to search for different conformers. The OPLS (OPLS_2005, Schrödinger, USA) force field was applied to geometrically optimize the ligand structure and to compute partial atomic charges. Finally, 32 poses per ligand were generated with different steric features for subsequent docking studies.

2.3.3. Molecular Docking—The prepared X-ray crystal structures of PCSK9 were used to generate receptor energy grids applying the default value of the protein atomic scale (1.0 Å) within the cubic box centered on the PCSK9 crystal structure interface at which it interacts with LDLR. PS was then docked using the Glide 5.8 module (Glide, version 5.8, 2012, Schrödinger, USA) in extra-precision (XP) mode.

2.4. Surface Plasmon Resonance

The recombinant human PCSK9 protein (ab198471, Abcam, Cambridge, MA, USA) was immobilized on the carboxymethylated dextran matrix of the sensor chip (Reichert) by using a standard primary amine coupling reaction on a Reichert Technologies SPR instrument (SR700DC, Buffalo, NY, USA) in 10 mM acetate buffer at pH 6.0. Free carboxyl groups on the surface were modified by injecting a mixture of 0.1 M 1-ethyl-3-(3-dimethylaminopropyl) carbodiimide hydrochloride (EDC) and 0.05 M *N*-hydroxysuccinimide (NHS) at a flow rate of 10 µL/min. The running buffer was 0.01 M PBS, 0.138 M NaCl, 0.0027 M KCl, and 0.05% Tween 20 at pH 7.4. After the immobilization, the unreacted activated groups were blocked with 1M ethanolamine (pH 8.5) for 7 min. After immobilization, different concentrations (10 to 150 µM) of PS were injected for binding to PCSK9 protein over the sensor chip surface at 25 °C, with a flow rate of 25 µL/min. The surface was regenerated after each experiment by removing the bound compound with glycine at pH 2.2. The goldenseal (*Hydrastis canadensis*) isoquinoline alkaloid berberine (Alfa Aesar, Tewksbury, MA, USA) was used as a negative control.

For competitive analysis, recombinant human LDLR protein (ab220570, Abcam, Cambridge, MA, USA) was immobilized as discussed earlier with 10 mM acetate buffer at pH 4.5. The sensor chip surface was modified with the amine coupling and blocking was done with 1M ethanolamine (pH 8.5) like the previous experiment. After immobilization, different concentrations of PS were mixed with fixed amount of PCSK9 (200 nM) in running buffer and were injected over the sensor chip surface at a flow rate of 25 µL/min to evaluate the competitive binding of PS to LDLR protein in presence of PCSK9. The surface was regenerated after each experiment with glycine pH 2.2. Berberine (100 µM), used as a negative control, was mixed with PCSK9 (200 nM) and injected over the sensor chip.

2.5. Cell Lines and Culture Conditions

Human breast cancer cell line BT-474 (luminal B/ER⁺, PR⁺, and HER-2⁺) and T47D (luminal A/ER⁺, PR⁺, and HER-2⁻) were purchased from the American Type Culture Collection (ATCC, Rockville, MD, USA). Cells were cultured and maintained as previously described [29].

2.6. In Vitro Studies

2.6.1. Experimental Treatment—PS was dissolved in dimethyl sulfoxide (DMSO) to provide a final 25 mM stock solution, which used to prepare various concentrations of treatment media. The final concentration of DMSO was maintained fixed in all treatment groups within a given experiment and never exceeded 0.1% of each.

2.6.2. Cell Viability Assay—Cells were seeded into a 96-well plate at a density of 5×10^3 cells/well (6 replicates/group) in Roswell Park Memorial Institute (RPMI)-1640 media supplemented with 10% fetal bovine serum (FBS) and allowed to attach overnight. Next day, cells were divided into different treatment groups and exposed to respective control or experimental treatments with various concentrations of PS for 24 h, 48 h, and 72 h. At the end of treatment duration, the viable cell number was determined using 3-(4,5-dimethylthiazol-2-yl)-2,5-diphenyl-tetrazolium bromide (MTT) assay [29]. MTT was added to each well at a final concentration of 1.0 mg/mL. After 3 h incubation at 37 °C, media was removed, and formazan crystals were dissolved in DMSO (100 μ L/well). Optical density was measured at 570 nm on a microplate reader (BioTek, Winooski, VT, USA). The number of cells/well was calculated against a standard curve prepared by plating various numbers of cells at the start of each experiment.

2.7. Western Blot Analysis

BC cells were initially plated at 1×10^6 cells/100 mm culture plates in RPMI-1640 media supplemented with 10% FBS and allowed to adhere overnight. Cells were then washed with phosphate buffered saline (PBS) and treated with the respective control or treatment media containing various concentrations of PS for 72 h. Cells were then harvested and washed twice with cold PBS, re-suspended and lysed in Radioimmunoprecipitation assay (RIPA) buffer (Qiagen Sciences Inc., Valencia, CA, USA) at 4 °C for 30 min. Lysates were centrifuged for 10 min at 14,000 \times g and supernatants were stored at -80 °C as whole cell extracts. For animal tissues (tumor and liver), Dulbecco's phosphate buffered saline (DPBS) was prepared as 1 mL DPBS in 10 μ L protease inhibitor. Samples were weighted and added in equivalent weights to DPBS (1 mg sample/5 μ L DPBS) and homogenization was conducted using ultrasonic homogenizer (Qsonica Sonicator, Newtown, CT, USA). Each homogenate was re-suspended and lysed in RIPA buffer at 4 °C for 30 min. Lysates were centrifuged for 10 min at 14,000 \times g and supernatants were stored at -80 °C. Protein concentration was determined by the Pierce BCA Protein Assay (Bio-Rad, Hercules, CA, USA). Protein concentration of lysates were loaded as cell lysate 20 μ g, liver lysate 7 μ g, and tumor lysate 15 μ g. Proteins were separated on 8% sodium dodecyl sulfate polyacrylamide gel electrophoresis (SDS-PAGE) gels and transferred to polyvinylidene difluoride membranes. Membranes blocked with 5% bovine serum albumin (BSA) in 10 mM Tris-HCl containing 50 mM NaCl and 0.1% Tween 20, pH 7.4 (TBST), and incubated with the indicated primary antibodies overnight at 4 °C. Membranes were washed 5 times with TBST and then corresponding horseradish peroxidase-conjugated secondary antibodies were used against each primary antibody for 1 h at room temperature, followed by rinsing with TBST, 5X. Proteins were detected using ChemiDoc XRS chemiluminescent gel imaging system and analyzed using Image Lab software (Bio-RAD, Hercules, CA, USA).

[29]. Visualization of β -actin was used to ensure equal sample loading in each lane. Experiments were repeated two times and representative images are presented in figures.

2.8. In Vivo Studies

2.8.1. Animals—Female athymic nude mice (Foxn1^{nu}/Foxn1⁺, 5–6 weeks old) were purchased from Envigo (Indianapolis, IN, USA). Animals were housed at the Animal Facility (College of Pharmacy, University of Louisiana at Monroe) and maintained under clean conditions in sterile filter-top cages, at a temperature of 24±2 °C, 50%±10% relative humidity, and 12:12 h artificial light–dark cycle. Mice received either Teklad S-2335 Mouse Breeder Sterilizable Diet (total fat 11.4%, crude proteins 17.2%, and carbohydrates 45.2%) or Teklad LM-485 (total fat 5.8%, crude proteins 19.1%, and carbohydrates 44.3%) and water ad libitum. All procedures were conducted in accordance with the recommendations in the Guide for the Care and Use of Laboratory Animals of the National Institutes of Health and with the approval by the Institutional Animal Care and Use Committee (IACUC), protocol# 18FEB-KES-01.

2.8.2. Comparison of in vivo HER2⁺/ER⁺ BC Growth Using Regular and High Fat Diets in Athymic Nude Mouse Model—Ten athymic female nude mice were divided into two groups, (n=5, each). Group-1 fed a regular chow diet (Teklad LM-485), while group-2 fed a high fat diet (Teklad S-2335). One week later, all mice were subcutaneously xenografted 5 × 10⁶ BT-474 cells, the HER2⁺/ER⁺ BC cells, at the 2nd mammary fat pad. Tumor volume was monitored every-other-day with a digital caliber (VWR, Radnor, PA, USA). One week after xenografting, tumors started to become palpable. Experiment terminated on day-28, mice sacrificed, and tumors volume and weight were calculated.

2.8.3. In Vivo Effects of PS on The HER2⁺/ER⁺ BC Growth and Recurrence After Primary Tumor Surgical Excision in Nude Mouse Xenograft Model—Mice were randomized to vehicle control and PS-treated groups (n=5 per group). One week before tumor cells xenografting, animals received PS 10 mg/kg orally daily (dissolved in 0.2% DMSO in PBS) or vehicle control, which continued until the experiment termination. Seven days after first dose, BT-474 cells (3-5 passages) were washed with and re-suspended in serum free RPMI-1640 medium. Cell suspension (5 × 10⁶ cells in 50 μ L per mouse) was injected at the 2nd mammary fat pad of each nude mouse, using a 29G hypodermic needle. Mice were observed daily for the growth of palpable tumors at the site of injection. Seven days post implantation; tumors became visible with an approximate average volume of 50 mm³. It took additional 15 days for the generated tumors in vehicle-treated control mice to reach the average volume of 1,000 mm³. Primary tumors were then surgically excised in both animal groups and excised tumors were stored frozen at –80 °C. Xenografted mice were anesthetized prior to the surgical excision procedure using ip ketamine/xylazine combination (100 mg/kg-15 mg/kg). After 15–20 min of injecting the anesthetic, animal reflexes were tested by gently tapping the hind legs with a sterile syringe needle, and when animals were fully anesthetized, their primary tumors were surgically excised, and each wound was closed by one or two stitches. Ketoprofen, 1 mg/kg, was used 12 h before and after surgery for effective analgesia. Ophthalmic lubricant was used during the surgery to

prevent corneal drying. Bupivacaine (0.25%, 1–2 drops), twice daily, was used topically at the excision wound site to prevent local infiltration along the surgery site during closure, with a maximum dose of 2 mg/kg. One day after surgical excision of the primary breast tumors, animals which originally treated with vehicle control continued the same treatment while mice treated with PS continued the same 10 mg/kg, oral, 7X/week treatment. Mice were observed regularly to assure post-surgery wounds healing and contamination-free. Treatments continued for additional 30 days. Mice were then sacrificed at the indicated time, unless they appeared to be moribund or tumor volume exceeded 1,800 mm³, at which they were immediately sacrificed. The mice were monitored daily for new tumors and body weight, and carefully observed for general health characters, including food and water intake, defecation, urination, and physical activity. Tumor dimensions were measured every two days using a digital caliber. Tumor volume was calculated using the well-established formula: tumor volume (mm³) = [(length × width²)/2]. At the end of the experiment, mice were sacrificed, and fresh blood samples were collected in heparinized microtainer tubes. Blood was immediately centrifuged at 4 °C at 13,000 rpm for 10 min to prepare plasma samples, which were then stored at –80 °C until quantification of cancer antigen 15-3 (CA 15-3), estradiol, and total cholesterol. Collected tumors and organs were weighed and stored at –80 °C until total protein extraction for Western blot analysis.

2.9. Assessment of PS Effects on the Total Plasma Cholesterol Level

PS-treated and vehicle control mice total plasma cholesterol samples were assessed using cholesterol, total Cell Biolabs colorimetric assay kit (Cell Biolabs Inc., San Diego, CA), according to manufacturer's instructions.

2.10. Assessment of PS Effects on the 17β-Estradiol Plasma Level

PS-treated and vehicle control mice plasma samples were analyzed for the level of 17β-estradiol using estradiol enzyme-linked immunosorbent assay (ELISA) kit (Catalog Number 582281) from Cayman Chemical Company (Ann Arbor, MI, USA). Estradiol levels were measured according to manufacturer instructions.

2.11. Effects of PS Treatment on The Plasma Levels of the BC Recurrence Marker CA 15-3

The effect of PS on the human BC recurrence marker was assessed using Abnova CA 15-3 (human) ELISA Kit (Catalog Number KA0206). CA 15-3 levels were measured according to manufacture instructions.

2.12. Immunohistochemistry (IHC) study

IHC was performed on 10% formalin-fixed for 24 h, paraffin-embedded tumor tissue samples, cut into 5 μm-thick sections. Sectioning has been conducted at the AML Laboratories (Jacksonville, FL, USA). The sections were deparaffinized with xylene (3 times, 5 min each), rehydrated in a descending ethanol series (100% for 5 min; 100% for 5 min; 95% for 5 min; 95% for 5 min; 70% for 5 min; 50% for 5 min; and 30% for 5 min), and 2 times by distilled water for 5 min. This was followed by antigen retrieval with citrate unmasking solution (1X) (Catalog Number 14746, Cell Signaling Technology, Beverly, MA, USA) of pH 6.0, microwaved on high power until boiling is initiated; followed by 10 min at

a sub-boiling temperature (95°C). Sections were kept cooling down on bench for 30 min. Sections were washed with distilled water and incubated with 3% H₂O₂ (Fisher Scientific, Waltham, MA, USA) for 10 min. Sections were washed using 1X Tris buffered saline (Bio-Rad, Hercules, CA, USA) with Tween® 20 (TBST). Later, sections were incubated in blocking buffer, TBST in 10% normal goat serum (Cell Signaling Technology, Beverly, MA, USA) for 1 h at room temperature. Sections were then incubated with the primary antibodies overnight at 4 °C: PCSK9 and LDLR each at a dilution of 1:200. On the next day, sections were washed 3X with TBST buffer and incubated in boost IHC detection reagent (Cat # 8114S, Cell Signaling Technology, Beverly, MA, USA) for 30 min at room temperature. This was followed by buffer washing, the polymeric detection system, DAB detection kit (Cat # 8059S, Cell Signaling Technology, Beverly, MA, USA) was used according to manufacturer's protocol. Finally, the sections were counter-stained with hematoxylin (Cell Signaling Technology, Beverly, MA, USA) at room temperature for 1 min. Sections were dehydrated through 95% ethanol, absolute ethanol, and xylene. Sections were then cover-slipped with mounting media (Cell Signaling Technology, Beverly, MA, USA).

2.13. Hematoxylin and Eosin Y (H&E) Staining

Different organ tissues were freshly collected and immediately fixed in 10% neutral buffered formalin for 48 h. The tissues were further transferred to 70% ethanol, processed, and embedded in paraffin. All the sectioning and H&E staining has been conducted at the AML Laboratories. Briefly, paraffin-embedded tissues were sliced into 5 µm sections and mounted on positively charged slides, dewaxed with xylene, rinsed with alcohol, rehydrated by water, and finally, the tissue slides were stained with H&E. Tissues were then dehydrated by ethanol and xylene and then cover slipped with mounting media as described earlier in IHC method.

2.14. Statistics

Results are presented as the mean ± standard error of the mean (SEM) of at least two independent experiments. Differences between two groups (control vs. treatment) were determined by Student's two-tailed t-test. Differences between three or more groups (control vs. different treatment concentrations) were determined by one-way analysis of variance (ANOVA) followed by post hoc analysis Dunnett's test. All statistics done using GraphPad Prism software version 8 (La Jolla, CA, USA). A difference of * p <0.05, ** p<0.01, *** p<0.001, and **** p<0.0001 was considered statistically significant, compared to the vehicle-treated control group.

3. Results

3.1. Effects of PS on the Secretion of PCSK9 in vitro

The Eli Lilly's PD²/OIDD Program screened a small in-house natural products library for ability to inhibit the PCSK9 secretion in HepG2 cells. Of these, PS showed PCSK9 secretion inhibitory activity in 3-effort levels. PS inhibited the expression of PCSK9 in HepG2 cells, with an IC₅₀ value of 1.2 µM (Figure S1). In Huh-7 cells, 5 µM of PS inhibited 31.2% of PCSK9 secretion (data not shown). PS didn't cause cytotoxicity or affected HepG2 or Huh-7 viability even at doses >50 µM. Berberine and its analogs were the only natural products that

have previously been shown to suppress PCSK9 secretion [30,31], but they did not affect its protein-protein interactions.

3.2. In-Silico Binding of PS at The PCSK9-LDLR Interaction Interface

A predictive molecular modeling study was conducted using Schrödinger software to assess the ability of PS to interfere with PCSK9-LDLR interaction at their binding interface. The available wild-type PCSK9 crystal structures PDB codes 4NE9, 4NMX, and 3GCW and the mutant-type PCSK9 crystal structure PDB code 3GCX were used (Figure 1 and Figures S2 and S3). Interestingly, PS was able to accommodate the PCSK9 catalytic domain that is usually occupied by the EGF-A domain of the LDLR in all investigated crystal structures (Figure S2). PS showed an average docking score of -7.0 , with a good RMSDs average of 0.2 \AA . PS afforded the conformational flexibility needed to fit into the shallow PCSK9 catalytic domain and provided proper molecular size necessary for adequate fitting. PS formed 3-5 hydrogen bonding (HB) interactions in all the wild-type PCSK9 crystal structures (Figure S2). PS maintained a critical HB interaction with the side chain of PCSK9 ASP374 in all investigated crystal structures (Figure S2). It was previously shown that HIS306 in the EGF-A domain of LDLR is involved in a salt bridge interaction with ASP374 in PCSK9 at low pH, enhancing the binding affinity [14]. The ability of PS to form a HB interaction with the PCSK9 ASP374 instead of the salt bridge should cause a pH-independent increase in the binding affinity towards PCSK9, mimicking the HIS306-Y substitution in either LDLR EGF-A or EGF-AB domains, which was previously reported [32].

Berberine was docked using the same PCSK9 crystal structures under the same docking parameters used to dock PS (Figure S3). Interestingly, berberine didn't show any interactions within the PCSK9 interface, and had a poor docking score of -3.1 , compared to PS. This clearly highlighted the structural uniqueness of PS, which enabled its perfect binding alignment at the narrow PCSK9-LDLR EGF-A binding pocket.

3.3. Surface Plasmon Resonance Validation of PS Ability to Inhibit PCSK9-LDLR Interaction

A surface plasmon resonance (SPR)-aided study was performed to assess the PS ability to bind at the PCSK9 and inhibiting its interaction with LDLR. PCSK9 (Abcam, ab221019) was immobilized on a carboxymethylated dextran sensor chip using 10 mM acetate buffer at pH 6.0. After immobilization, different concentrations ($10\text{-}150 \text{ \mu M}$) of PS injected onto the surface of sensor chip. Results suggest that PS dose dependently binds at PCSK9 (Figure 2A). A concentration-dependent kinetic study indicated that PS effectively binds PCSK9 protein with a K_d value of 23.4 \mu M . All binding kinetic analysis were calculated using the Tracedrawer Program (Ridgeview Instruments AB).

For competitive protein-protein interaction (PPI) inhibition analysis, the LDLR protein was immobilized onto a sensor chip. Different concentrations of PS were then mixed with fixed amount of PCSK9 protein (200 nM) in the running buffer and were injected over the sensor chip surface to evaluate the PS competitive PPI to the LDLR binding with PCSK9. The response dose-dependently decreased with the PS concentration increase (Figure 2B). Thus,

PS was able to inhibit the LDLR binding interaction with PCSK9. Berberine was used as a negative control [30,31], and consistent with *in silico* results, it didn't inhibit the PCSK9-LDLR interaction (Figure 2B).

3.4. Effects of PS on The Viability of the Hormone-Dependent BC Cells *in vitro*

The anti-proliferative activity of PS was evaluated against BT-474 and T47D cells, representing ER⁺, PR⁺-positive BC cell lines (Figure 3). PS treatments showed weak but time and dose-dependent inhibition of the growth of BT-474 and T47D BC cells, with gradual decrease of the IC₅₀ values over time (Table 1). PS was slightly more potent against BT-474 than T47D BC cells.

3.5. Effect of PS on The PCSK9 and LDLR Expression Levels in Hormone-Dependent BC Cells

The effect of different PS treatments on the expression levels of PCSK9 and LDLR in BT-474 and T47D BC cell lines was studied. Both BC cell lines treated with different doses of PS (25 μM, 50 μM, and 100 μM) for 72 h, followed by subsequent Western blot analysis of the expression levels of PCSK9 and LDLR. PS treatments significantly suppressed the PCSK9 level in a dose dependent manner compared to vehicle control in both BC cell lines (Figure 4). The PCSK9 level reduction was 8%, 36%, and 70% for PS treatments of 25 μM, 50 μM, and 100 μM, respectively, in comparison to vehicle-treated control in BT-474 cells (Figure 4A). Meanwhile in T47D cells, the PCSK9 level reduction was 22%, 40%, and 52% for PS treatments of 25 μM, 50 μM, and 100 μM, respectively, compared to the vehicle-treated controls (Figure 4B). Simultaneously parallel to the PCSK9 level reduction, the LDLR level was significantly increasing in a dose dependent manner, compared to vehicle-treated controls in both BC cell lines. In BT-474 cells, the level increase of LDLR level was 39%, 71%, and 100% for PS 25 μM, 50 μM, and 100 μM treatments, respectively, versus vehicle-treated controls (Figure 4A). In T47D cells, the LDLR level increase was 45%, 72%, and 210% for PS treatments of 25 μM, 50 μM, and 100 μM, respectively, compared to the vehicle-treated controls (Figure 4B).

3.6. Comparison of The Effects of High Fat Versus Regular Chow Diet on The Progression of BT-474 BC in Orthotopic Athymic Nude Mouse Model

A study was conducted to compare the effect of using high fat diet (HFD) versus regular chow diet on the HER2⁺/ER⁺ BC growth in athymic female nude mouse model. The mean tumor volume was $349.66 \pm 26.83 \text{ mm}^3$ for the mice fed on regular chow diet (5% fat). The mean tumor volume was $1180.35 \pm 153.75 \text{ mm}^3$ for mice fed HFD (11% fat), nearly 3.4-fold higher than that of regular diet (Figure 5A). The HFD fed group showed significant increase in the mean tumor weight, $1.334 \pm 0.101 \text{ g}$, compared to the regular diet fed group, which showed a mean tumor weight of $0.994 \pm 0.102 \text{ g}$ (Figure 5B). The HFD increased the tumor weight by 1.3-fold, compared to mice fed on regular chow diet.

3.7. Comparison of The Effect of High Fat Diet Versus Regular Chow Diet on The Expression of PCSK9 and LDLR in the HER2⁺/ER⁺ BT-474 BC Cells

The effect of diet on the expression of PCSK9 and LDLR proteins was studied by immunohistochemistry (IHC) of the collected BT-474 primary tumors orthotopically xenografted in nude mice fed on regular chow diet (5% fat) or high fat diet (11% fat) (Figure 6). Data showed that mice fed high fat diet have strong and highly differentiated expression of PCSK9 and LDLR levels in BT-474 hormone dependent BC tissue in compare to mice fed regular chow diet (Figure 6).

3.8. Effects of PS on Progression of HER2⁺/ER⁺ BC in Nude Mouse Xenograft Model

Parallel to the previous experiment, the antitumor activity of 10 mg/kg daily oral PS was assessed in HFD-fed orthotopic athymic mice bearing BT-474 tumor cells xenograft model. Previous experiment HFD-fed group was used as a vehicle control group. PS-treated mice showed a mean tumor volume of $474.07 \pm 105.43 \text{ mm}^3$ versus the previously reported $1,180.35 \pm 153.75 \text{ mm}^3$ vehicle-treated control mice (Figure 7B). PS treatment significantly suppressed the growth of BT-474 tumors by 59.8%, compared to the vehicle control group. The mean tumor weight was $1.334 \pm 0.101 \text{ g}$ and $0.956 \pm 0.119 \text{ g}$ for vehicle-control and PS-treated animals, respectively, (Figure 7C). The mice mean body weight in vehicle control and PS-treated groups was not significantly different over the experiment course (Figure 7D).

3.9. Immunohistochemical Comparison of The Effect of PS Treatment on The Expression of PCSK9 and LDLR in HER2⁺/ER⁺ Breast Tumor Tissues versus Vehicle Control

IHC study was conducted to study the effects of 10 mg/kg daily oral PS treatment on the expression of PCSK9 and LDLR proteins in HFD fed nude mice bearing BT-474 hormone dependent BC as it compared to vehicle-treated controls. Results showed that the PS treatment reduced the expression level of PCSK9 compared to vehicle control group (Figure 8). The expression level of LDLR showed no-significant variations between PS and vehicle control treatments (Figure 8).

3.10. Effects of PS Treatment on Locoregional Recurrence of HER2⁺/ER⁺ BC in Nude Mouse Xenograft Model

To further investigate the potential of PS as an inhibitor for breast tumor locoregional recurrence, oral PS treatment was continued for additional four weeks after primary tumor surgical resection. Three out of five mice in the vehicle-treated control group developed recurrence tumors on the 38th day of the study, while only two of the five PS-treated mice developed recurrence tumors on the 44th day of the study (Figure 9). The mean tumor volume for the vehicle-treated control mice was $793.41 \pm 729.19 \text{ mm}^3$, compared to $171.33 \pm 133.79 \text{ mm}^3$ for PS-treated mice group, representing 78.4% suppression of the tumor recurrence (Figure 9C). The mean recurrence tumor weight at the study end for the vehicle-treated control group was $1.7 \pm 0.56 \text{ g}$ versus $0.36 \pm 0.27 \text{ g}$ for the PS-treated group animals (Figure 9D). Worth mentioning, a mouse among the vehicle-treated control was sacrificed on the 49th day of the study due to reaching the maximum tumor volume allowed by the experiment protocol ($1,800 \text{ mm}^3$). No statistically significant difference in animals

body weight was observed between PS-treated and vehicle control-treated groups at any given time point over the study duration (Figures 9E).

3.11. Effects of PS Treatment on The Expression Levels of PCSK9 and LDLR in Liver and Tumor Tissues

The *in vivo* effects of PS treatment on the expression of PCSK9 and LDLR were studied by Western blot analysis of the collected primary and recurred tumors and nude mouse livers (Figure 10). Analysis of the nude mice liver lysates showed 30% reduction of the PCSK9 expression level and 109% increase of the LDLR level in PS-treated mice compared to vehicle-treated controls (Figure 10A). The excised primary tumor lysates also showed 70% reduction of the PCSK9 expression level without significant change of the LDLR level in PS-treated mice tumors versus vehicle-treated controls (Figure 10B). Similarly, analysis of the recurred tumor lysates showed 62% reduction of the PCSK9 expression level and stabilized LDLR level in PS-treated mice compared to vehicle-treated controls (Figure 10C).

3.12. Effect of PS on Nude Mice Plasma Total Cholesterol Levels

PS-treated mice had no statistically significant decrease in plasma total cholesterol levels for PS treatment (131.21 ± 10.77 mg/dL) compared to vehicle control treatment (144.26 ± 11.93 mg/dL), which represents 9.0% reduction in cholesterol level for PS-treated group (Figure 11A).

3.13. Effects of PS on Nude Mice Plasma 17 β -Estradiol Level

The 17 β -estradiol levels were measured in nude mouse plasma after the study end. PS treatment group showed 10.3% 17 β -estradiol level decrease, which was not a statistically significant reduction compared to vehicle control-treated animals (Figure 11B).

3.14. Effects of PS Treatment on The Plasma Level of The BC Recurrence Marker CA 15-3

Cancer antigen 15-3 (CA 15-3) is a reliable marker for human BC recurrence that was measured in nude mouse plasma at the experiment end. The plasma levels of CA 15-3 were significantly higher in vehicle control-treated animals, 1.64 ± 0.39 U/mL, compared to PS-treated mice, 0.37 ± 0.08 U/mL, representing 77.4% reduction of the recurrence biomarker CA 15-3 in treatment group (Figure 11C).

3.15. Histopathological effects of PS Treatment on Collected Tumor Tissues

Histological investigation of collected primary tumors showed moderately to poorly differentiated tumor cells, which exhibit glandular pattern with areas of necrosis more abundant in treatment group (Figure S4). Tumor cells exhibit hyperchromatic, pleomorphic nuclei with high proliferative mitotic figures. There was no significant variation between the PS and vehicle control-treated tumor histology. Recurrent tumors exhibit pattern similar to the primary tumors, but the PS-treated recurred tumors have larger areas of necrosis (Figure S4).

3.16. Potential PS Treatment Toxicity on Different Mice Organs

The PS 10 mg/kg daily oral dose produced no gross adverse and/or behavioral responses in female athymic nude mice over previously described experiment periods. PS-treated mice showed no significant change in collected various organs' weight compared to vehicle control (Table S1). The collected organs including the brain, heart, lung, liver, spleen, and kidney were sectioned and stained to study any histopathological changes or tumor metastatic pattern (Figures S5 and S6). No metastatic foci observed in any organ neither in vehicle control nor in treated organs (Figure S5). No histopathological changes observed in organs except in liver sections, which showed microvesicular steatosis in both control and PS-treated liver mice (Figure S6). The microvesicular steatosis is characterized by small intracytoplasmic fat vacuoles, which accumulate within the hepatocyte and considered a typical pathological pattern in nude mice fed on HFD for longer than 9 weeks [33,34].

4. Discussion

The Cancer Genome Atlas proved the key role of overexpression of cholesterol synthesis genes play in various malignancies, including BC [5]. Cholesterol is a starting biosynthetic precursor for steroidogenesis, which can lead to the biosynthesis of 17β -estradiol, an estrogen receptor agonist, which activates several signaling pathways in hormone dependent BC. Therefore, hypercholesterolemia correlates well with aggressive hormone-dependent BC profile [35,36]. Circulating PCSK9 binds LDLR, preventing the recycling of this receptor through binding with LDL and targeting the receptor for lysosomal compartment leading to its degradation, which promotes hypercholesterolemia [37]. Several studies correlated overexpressed PCSK9 with hypercholesterolemia and multiple malignancies [37–39]. A nanoliposomal anti-PCSK9 vaccine showed anti-tumor effect in mice bearing colorectal cancer [40]. Another anti-PCSK9 vaccine also showed potential anti-BC effects in an experimental model [41]. A Mendelian randomization study correlated reduced LDL-C due to PCSK9 variants with reduced BC risk [42]. Elevated PCSK9 serum level proved a prognostic marker in advanced non-small cell lung cancer patients [43]. PCSK9 enhanced the metastasis of B16F1 melanoma cells to liver, and this effect was significantly abolished when PCSK9 was knocked down in a mouse model [38]. PCSK9 is expressed mainly in liver [37] and CNS [38], which are the common sites for subsequent tumor metastasis in different solid cancers [38,44,45]. Compared to normal human mammary epithelial cells, BC cells have increased cholesterol content and many of them overexpress PCSK9 [46]. Cholesterol accumulation is likely due to the change in cholesterol acquisition, efflux and/or transport within the BC cells [46]. Metastasis of BC has been significantly enhanced with cholesterol-enriched diet in animal models [7]. BC cells require higher cholesterol levels to invade the circulatory systems [7,46,47]. No previous attempts explored the effects of PCSK9 inhibitors to control hypercholesterolemia-induced BC progression and recurrence.

The initial discovery of PS PCSK9 secretion-reducing activity in HepG2 and Huh-7 hepatocellular carcinoma cells was through data acquired by Eli Lilly's OIDD Program (Figure S1)[48]. Molecular modeling data suggested the potential of PS to interfere with the PCSK9-LDLR protein-protein interaction (Figures 1B and S2). This effect was subsequently confirmed by surface plasmon resonance (SPR) [49]. SPR is a valid technology to study the

protein-protein interactions, their rates, kinetics, and intermolecular binding affinities [49]. SPR data proved PS bind PCSK9 at the same site, which accommodate EGF-A domain of LDLR (Figure 2). Therefore, PS inhibited PCSK9 interaction with LDLR in a dose-dependent manner, unlike berberine, the natural product that proved suppressing PCSK9 secretion, but failed to inhibit the PCSK9-LDLR interaction [30,31]. This activity variation may be due to the PS optimal molecular size and unique pharmacophoric features compared to berberine. PS showed a dose-dependent modest *in vitro* anti-proliferative activity against the luminal A T47D and the luminal B BT-474 hormone dependent BC cell lines, with IC₅₀ near 100 μM over 72 h treatment exposure. PS suppressed the *in vitro* PCSK9 expression levels in T47D and BT-474 BC cells a dose-dependent manner. The selection of treatment dose for this experiment was based on the PS IC₅₀ values in viability assays, using the highest treatment dose and two other lower doses representing 50% and 25% of the PS MTT assay IC₅₀ values. Treatment period also used 72 h because it is evident that PS needs a longer time to exert its PCSK axis targeting effects. PS also increased the levels of LDLR in a dose-dependent manner in both cell lines. These results suggested that the activity of PS is via dually targeting the PCSK9 secretion as well as inhibiting its protein-protein interactions with LDLR in BC cells. The modest *in vitro* cytotoxic activity against BC cell lines should not diminish the enthusiasm in PS because it showed potent *in vivo* activities especially against the BC recurrence. Low PS cytotoxicity can actually be advantageous for its plausible long-term use to prevent tumor recurrence by BC survivors with minimal expected off-target effects.

The luminal B BC BT-474 cell line was selected to study the *in vivo* anticancer activity of PS because this cell line represents an aggressive phenotype of the hormone-dependent (ER⁺ and PR⁺) and HER2⁺ BC and was more sensitive than T47D cells in MTT assay. Several studies demonstrated the association between the high fat diet (HFD) with aggressive BC [5–7]. This study showed that the HFD, 11% fat contents, enhanced the progression of BT-474 cell tumors in an orthotopic nude mouse model, compared to mice fed regular chow diet (5% fat). The IHC study of the BT-474 cells collected tumors showed that the HFD fed mice had higher PCSK9 and LDLR expression levels and differentiation within the tumor tissue compared to tumors collected from mice fed on regular chow diet. Therefore, all subsequent *in vivo* experiments used HFD. In BC growth model, PS treatment effectively reduced BT-474 tumor growth by nearly more than 59% in an orthotopic nude mouse xenograft model versus vehicle control, validating the concept of targeting the PCSK9 pathway as a novel direction to control hormone-sensitive BC progression.

Recurrence is the leading cause of cancer patients' death, representing a major therapeutic challenge to oncologists. Although several therapeutic options are available for ER⁺BC, effective recurrence inhibitors are lacking. Neoadjuvant and adjuvant therapies have limited cancer recurrence preventive activity as they usually fail to eradicate residual quiescent tumor cells and actually some of them can induce recurrence by promoting extracellular vesicles [50]. We recently established a new model to assess BC locoregional recurrence in experimental nude mice [50]. In this model, tumor cells were orthotopically inoculated into nude mouse mammary fat pads to grow primary tumors, which were then surgically excised, and treatments can begin before or after the surgery to assess the ability of treatments to prevent or suppress the tumor recurrences [50]. Results from this study showed that oral

daily PS for 4 weeks suppressed more than 78% of the development of locoregional recurrence BT-474 cell tumors in most animals after primary tumor surgical excision. It is well-documented that every 2.6 adult mouse days are equivalent to one human year [51]. Therefore, the 6 days tumor recurrence onset delay in mice caused by PS treatment can be equivalent to 2.3 years tumor-free survival in humans. Histopathological examination of collected primary and recurred tumors indicate that the PS treatments induced more tumor apoptosis compared to vehicle-treated control (Figure S4). These novel findings provide evidence for the potential of PCSK9-targeting molecules for use to control hormone-dependent BC progression and recurrence. Primary breast tumors surgical excision does not eliminate the potential of local, regional, and/or distant disease relapse [52]. Introducing PS as a first-in-class dual inhibitor of PCSK9 expression and PCSK9-LDLR interaction is expected to warrant future consideration of the PCSK9 axis as a valid molecular target to reduce the risk of BC recurrence, and thereby improve long-term patients' survival rate. It is worth noting the potent *in vivo* PS inhibitory effects on the PCSK9 levels in primary and recurrence tumors. PS treatment also normalized the level of LDLR in primary and recurrence tumors. Blocking the induction of PCSK9, indirectly reduced the degradation of LDLR and hence minimized the chance for the tumor cell ability to improve its cholesterol utilization. PS treatment also reduced the plasma total cholesterol level in mice. Undoubtedly, the availability of small molecule PCSK9-LDLR interaction inhibitor would be more convenient and cost-effective option compared to the current FDA-approved mAb drugs. The PS cost-effectiveness is based on its sustained fermentation supply source, and anticipated ease for commercial productions. In addition to targeting only extra-cellular PCSK9, off-target effects list for current FDA-approved humanized monoclonal antibodies include cardiovascular, gastrointestinal, genitourinary, hypersensitivity, musculoskeletal, nervous system, neurocognitive, respiratory, immunogenic, and others [53]. Western blotting results indicated that PS can also target intracellular PCSK9 in liver and tumor cells. PS also has other advantage versus mAb drugs including its longer shelf-life, and conveniently orally active. The only PCSK9-targeting natural product berberine and analogs only target PCSK9 secretion but not its protein-protein interaction. Berberine also is known to induce a wide range of interactions with drugs and can displace bilirubin from albumin, increasing total and unbound bilirubin concentrations [30,31,54,55]. Over sixty days of PS therapeutic use, no significant change in animal body weight and their organs weights were observed. Histopathological examination of collected mice organs showed no abnormal pathological signs in PS-treated animal versus control group, suggesting potential preliminary safety. The observed microvesicular steatosis in liver sections of both control and treatment groups is likely attributed to the long-term use of HFD, which is a documented method to generate nonalcoholic fatty liver model in nude mice [33,34]. Additional future comprehensive toxicological studies are warranted. Cholesterol and its oxidized form 27-hydroxycholesterol are endogenous estradiol receptor modulators, which increase ER-mediated transcription of 17 β -estradiol responsive genes, contributing to hormone-dependent BC survival and progression [56,57]. Herein, PS treatment reduced the mice plasma 17 β -estradiol level, an effect that was apparently parallel to its anti-hypercholesterolemia, and likely correlate with tumor progression and recurrence suppression. Blood biomarkers play a key role for early diagnosis and prediction of future relapse and therapeutic responses [50,58]. The cancer antigen 15-3 (CA 15-3) is one of few reliable tumor markers for monitoring post-operative

risk of recurrence in cancer patients and considered superior over the carcinoembryonic antigen (CEA) for the early detection of BC recurrence [49,57]. PS treatment significantly reduced the CA 15-3 mice plasma level, which translate to reduced recurrence incidence for the PS-treated mice compared to the control animals. Collectively, this study validates pseurotins as a novel small molecule natural products class appropriate for the control of hormone-dependent BC.

5. Conclusion

The current study presents a first-in-class small molecule fungal metabolite, pseurotin A (PS), which dually reduced PCSK9 expression and prevented its interaction with LDLR, reducing the circulating cholesterol and suppressing the progression of hormone dependent BT-474 breast tumors in a nude mouse xenograft model. PS concomitantly reduced mice serum levels of 17 β -estradiol and the breast tumor recurrence marker CA 15-3. It also potently inhibited the locoregional BT-474 breast tumor cells recurrence after primary tumor surgical excision. Reduction of tumor recurrence was associated with the downregulation of PCSK9 level in recurred tumors. Targeting PCSK9 through inhibiting its expression and interaction with LDLR is a novel strategy to control hormone dependent breast malignancies. Although PS showed modest direct *in vitro* cytotoxic effect on tumor cells, induced optimum systemic hypocholesterolemia, and optimally inhibited tumor progression *in vivo*, it is very potent in suppressing BC recurrence when used for extended time. It significantly reduced PCSK9 expression levels in tumor cells, both *in vitro* and *in vivo*, suggesting it is acting both extracellularly and intracellularly unlike the current FDA-approved mAb drugs, which only act extracellularly.

Supplementary Material

Refer to Web version on PubMed Central for supplementary material.

Acknowledgements:

This work was supported by the Louisiana Biomedical Research Foundation Award Number 2017-18 BRF Seed Funding Program. The financial support of the Louisiana Biomedical Research Network through the National Institute of General Medical Sciences (NIGMS) Grant 8P20GM10342 is acknowledged. The Eli Lilly's Open Innovation Drug Discovery Program is acknowledged for biological assays.

References

- [1]. Siegel RL; Miller KD; Jemal A Cancer statistics, 2020. *CA Cancer J. Clin* 2020, 70, 7–30.
- [2]. Lu CW; Lo YH; Chen CH; Lin CY; Tsai CH; Chen PJ; Yang YF; Wang CH; Tan CH; Hou MF; Yuan SSF VLDL and LDL, but not HDL, promote breast cancer cell proliferation, metastasis and angiogenesis. *Cancer Lett.* 2017, 388, 130–138. [PubMed: 27940127]
- [3]. Guan X; Liu Z; Zhao Z; Zhang X; Tao S; Yuan B; Zhang J; Wang D; Liu Q; Ding Y Emerging roles of low-density lipoprotein in the development and treatment of breast cancer. *Lipids Health Dis.* 2019, 18. [PubMed: 30658647]
- [4]. White CP On the occurrence of crystals in tumours. *J. Pathol. Bacteriol* 1909, 13, 3–10.
- [5]. Kuzu OF; Noory MA; Robertson GP The role of cholesterol in cancer. *Cancer Res.* 2016, 76, 2063–2070. [PubMed: 27197250]

- [6]. McDonnell DP; Park S; Goulet MT; Jasper J; Wardell SE; Chang CY; Norris JD; Guyton JR; Nelson ER Obesity, cholesterol metabolism, and breast cancer pathogenesis. *Cancer Res.* 2014, 74, 4976–4982. [PubMed: 25060521]
- [7]. Huang J; Li L; Lian J; Schauer S; Vesely PW; Kratky D; Hoefler G; Lehner R Tumor-induced hyperlipidemia contributes to tumor growth. *Cell Rep.* 2016, 15, 336–348. [PubMed: 27050512]
- [8]. Gabitova L; Gorin A; Astsaturov I Molecular pathways: Sterols and receptor signaling in cancer. *Clin. Cancer Res.* 2014, 20, 28–34. [PubMed: 24158702]
- [9]. Banerjee Y; Santos RD; Al-Rasadi K; Rizzo M Targeting PCSK9 for therapeutic gains: Have we addressed all the concerns? *Atherosclerosis* 2016, 248, 62–75. [PubMed: 26987067]
- [10]. Abifadel M; Varret M; Rabès JP; Allard D; Ouguerram K; Devillers M; Cruaud C; Benjannet S; Wickham L; Erlich D; Derré A; Villéger L; Farnier M; Beucler I; Bruckert E; Chambaz J; Chanu B; Lecerf JM; Luc G; Moulin P; Weissenbach J; Prat A; Krempf M; Junien C; Seidah NG; Boileau C Mutations in PCSK9 cause autosomal dominant hypercholesterolemia. *Nat. Genet* 2003, 34, 154–156. [PubMed: 12730697]
- [11]. Wang Y; Liu ZP PCSK9 inhibitors: Novel therapeutic strategies for lowering LDL cholesterol. *Mini-Reviews Med. Chem* 2018, 19, 165–176.
- [12]. Bottomley MJ; Cirillo A; Orsatti L; Ruggeri L; Fisher TS; Santoro JC; Cummings RT; Cubbon RM; Surdo PL; Calzetta A; Noto A; Baysarowich J; Mattu M; Talamo F; Francesco RD; Sparrow CP; Sitlani A; Carfi A Structural and biochemical characterization of the wild type PCSK9-EGF(AB) complex and natural familial hypercholesterolemia mutants. *J. Biol. Chem* 2008, 284, 1313–1323. [PubMed: 19001363]
- [13]. Surdo PL; Bottomley MJ; Calzetta A; Settembre EC; Cirillo A; Pandit S; Ni YG; Hubbard B; Sitlani A; Carfi A Mechanistic implications for LDL receptor degradation from the PCSK9/LDLR structure at neutral pH. *EMBO Rep.* 2011, 12, 1300–1305. [PubMed: 22081141]
- [14]. Kwon HJ; Lagace TA; McNutt MC; Horton JD; Deisenhofer J Molecular basis for LDL receptor recognition by PCSK9. *Proc. Natl. Acad. Sci* 2008, 105, 1820–1825. [PubMed: 18250299]
- [15]. Pettersen D; Fjellström O Small molecule modulators of PCSK9—A Literature and patent overview. *Bioorg. Med. Chem. Lett* 2018, 28, 1155–1160. [PubMed: 29519739]
- [16]. Tachalertpaisam J; Zhao B; Liang X; Burgess K Small molecule inhibitors of the PCSK9•LDLR interaction. *J. Am. Chem. Soc* 2018, 140, 3242–3249. [PubMed: 29378408]
- [17]. Shan L; Pang L; Zhang R; Murgolo NJ; Lan H; Hedrick JA PCSK9 binds to multiple receptors and can be functionally inhibited by an EGF-A peptide. *Biochem. Biophys. Res. Commun* 2008, 375, 69–73. [PubMed: 18675252]
- [18]. Wenke J; Anke H; Sterner O Pseurotin A and 8-O-demethylpseurotin A from *Aspergillus fumigatus* and their inhibitory activities on chitin synthase. *Biosci. Biotechnol. Biochem* 1993, 57, 961–964.
- [19]. Komagata D; Fujita S; Yamashita N; Saito S; Morino T Novel neuritogenic activities of pseurotin A and penicillic acid. *J. Antibiot* 1996, 49, 958–959.
- [20]. Wink J; Grabley S; Gareis M; Thierecke R; Kirsch R Pseurotin F1/F2, new metabolites from *Aspergillus fumigatus*, process for their preparation and use as apomorphine antagonists 1992, Eur Patent 546474.
- [21]. Wink J; Grabley S; Gareis M; Zeeck A; Philipps S Biologically active pseurotin A and D, new metabolites from *Aspergillus fumigatus*, process for their preparation and their use as apomorphine antagonists 1992, European Patent 546475.
- [22]. Shi YS; Zhang Y; Chen XZ; Zhang N; Liu YB Metabolites produced by the endophytic fungus *Aspergillus fumigatus* from the stem of *Erythrophloeum fordii* Oliv. *Molecules* 2015, 20, 10793–10799. [PubMed: 26111169]
- [23]. Han XX; Xu XY; Cui CB; Gu QQ Alkaloidal compounds produced by a marine-derived fungus, *Aspergillus fumigatus* HI-04, and their antitumor activities. *Chin. J. Med. Chem* 2007, 17, 232–237.
- [24]. Copmans D; Rateb M; Tabudravu JN; Pérez-Bonilla M; Dirx N; Vallorani R; Diaz C; Palacio JPD; Smith AJ; Ebel R; Reyes F; Jaspars M; De Witte P Zebrafish-based discovery of antiseizure compounds from the Red Sea: Pseurotin A2 and azaspirofurane A. *ACS Chem. Neurosci* 2018, 9, 1652–1662. [PubMed: 29672015]

- [25]. Companas D; De White P; Ebel R; Jaspars M; Ny A; Rateb M; Smith A; Trabudravu J Treatment of epilepsy using pseurotins and azaspirofurans. PCT International Application 2019, WO 2019043019 A1 20190307.
- [26]. Chen K; Xu J; Liu Q; Zhao J; Yuan Y; Lin Q Pseurotin A inhibits osteoclastogenesis and prevents ovariectomized-induced bone loss by suppressing reactive oxygen species. *Theranostics* 2019, 9, 1634–1650. [PubMed: 31037128]
- [27]. Vasicek O; Fedr R; Skoroplyas S; Chalupa D; Sklená M; Tharra PR; Švenda J; Kubala L Natural pseurotins and analogs thereof inhibit activation of B-cells and differentiation into the plasma cells. *Phytomedicine* 2020, 69, 153194. [PubMed: 32146299]
- [28]. Olsson MHM Protein electrostatics and PKa blind predictions; contribution from empirical predictions of internal ionizable residues. *Proteins: Struct., Funct., Bioinf.* 2011, 79, 3333–3345.
- [29]. Siddique A; Ebrahim H; Akl M; Ayoub N; Goda A; Mohyeldin M; Nagumalli S; Hananeh W; Liu YY; Meyer S; Sayed KE (–)-Oleocanthal combined with lapatinib treatment synergized against HER-2 positive breast cancer in vitro and in vivo. *Nutrients* 2019, 11, 412.
- [30]. Cameron J; Ranheim T; Kulseth MA; Leren TP; Berge KE Berberine decreases PCSK9 expression in HepG2 cells. *Atherosclerosis* 2008, 201, 266–273. [PubMed: 18355829]
- [31]. Liu DL; Xu LJ; Dong H; Chen G; Huang ZY; Zou X; Wang KF; Luo YH; Lu FE Inhibition of proprotein convertase subtilisin/kexin type 9: A novel mechanism of berberine and 8-hydroxy dihydroberberine against hyperlipidemia. *Chin. J. Integr. Med* 2014, 21, 132–138. [PubMed: 24893659]
- [32]. Ni YG; Marco SD; Condra JH; Peterson LB; Wang W; Wang F; Pandit S; Hammond HA; Rosa R; Cummings RT; Wood DD; Liu X; Bottomley MJ; Shen X; Cubbon RM; Wang SP; Johns DG; Volpari C; Hamuro L; Chin J; Huang L; Zhao JZ; Vitelli S; Haytko P; Wisniewski D; Mitnaul LJ; Sparrow CP; Hubbard B; Carfi A; Sitalani A A PCSK9-binding antibody that structurally mimics the EGF(A) domain of LDL-receptor reduces LDL cholesterol in vivo. *J. Lipid Res* 2010, 52, 78–86. [PubMed: 20959675]
- [33]. Chiappini F; Desterke C; Bertrand-Michel J; Guettier C; Le Naour F Hepatic and serum lipid signatures specific to nonalcoholic steatohepatitis in murine models. *Sci. Reports* 2016, 6, 31587.
- [34]. Kanuri G; Bergheim I In vitro and in vivo models of non-alcoholic fatty liver disease (NAFLD). *Int. J. Mol. Sci* 2013, 14, 11963–11980. [PubMed: 23739675]
- [35]. Nelson ER; Chang CY; McDonnell DP Cholesterol and breast cancer pathophysiology. *Trends Endocrinol. Metab* 2014, 25, 649–655. [PubMed: 25458418]
- [36]. Pelton K; Coticchia CM; Curatolo AS; Schaffner CP; Zurakowski D; Solomon KR; Moses MA Hypercholesterolemia induces angiogenesis and accelerates growth of breast tumors in vivo. *Am. J. Pathol* 2014, 184, 2099–2110. [PubMed: 24952430]
- [37]. Canuel M; Sun X; Asselin MC; Paramithiotis E; Prat A; Seidah NG Proprotein convertase subtilisin/kexin type 9 (PCSK9) can mediate degradation of the low density lipoprotein receptor-related protein 1 (LRP-1). *PLoS ONE* 2013, 8.
- [38]. Sun X; Essalmani R; Day R; Khatib AM; Seidah NG; Prat A Proprotein convertase subtilisin/kexin type 9 deficiency reduces melanoma metastasis in liver. *Neoplasia* 2012, 14, 1122–1131. [PubMed: 23308045]
- [39]. Athavale D; Chouhan S; Pandey V; Mayengbam SS; Singh S; Bhat MK Hepatocellular carcinoma-associated hypercholesterolemia: Involvement of proprotein-convertase-subtilisin-kexin type-9 (PCSK9). *Cancer Metab.* 2018, 6. [PubMed: 29854399]
- [40]. Momtazi-Borojeni AA; Nik ME; Jaafari MR; Banach M; Sahebkar A Potential anti-tumor effect of a nanoliposomal anti-PCSK9 vaccine in mice bearing colorectal cancer. *Arch. Med. Sci* 2019, 15, 559–569. [PubMed: 31110520]
- [41]. Momtazi-Borojeni AA; Nik ME; Jaafari MR; Banach M; Sahebkar A Effects of immunization against PCSK9 in an experimental model of breast cancer. *Arch Med Sci.* 2019, 15, 570–579. [PubMed: 31110521]
- [42]. Nowak C; Arnlov J A Mendelian randomization study of the effects of blood lipids on breast cancer risk. *Nat. Comm* 2018, 9.
- [43]. Bonaventura A; Grossi F; Montecucco F PCSK9 is a promising prognostic marker in patients with advanced NSCLC. *Cancer Immun. Immunother* 2020, 69, 491–492.

- [44]. Zaid A; Roubtsova A; Essalmani R; Marcinkiewicz J; Chamberland A; Hamelin J; Tremblay M; Jacques H; Jin W; Davignon J; Seidah NG; Prat A Proprotein convertase subtilisin/kexin type 9 (PCSK9): Hepatocyte-specific low-density lipoprotein receptor degradation and critical role in mouse liver regeneration. *Hepatology* 2008, 48, 646–654. [PubMed: 18666258]
- [45]. Seidah NG; Benjannet S; Wickham L; Marcinkiewicz J; Jasmin S.; Stifani S; Basak A; Prat A; Chretien M The secretory proprotein convertase neural apoptosis-regulated convertase 1 (NARC-1): Liver regeneration and neuronal differentiation. *Proc. Natl. Acad. Sci. U. S. A* 2003, 100, 928–933. [PubMed: 12552133]
- [46]. Llaverias G; Danilo C; Mercier I; Daumer K; Capozza F; Williams TM; Sotgia F; Lisanti MP; Frank PG Role of cholesterol in the development and progression of breast cancer. *Am. J. Pathol* 2011, 178, 402–412. [PubMed: 21224077]
- [47]. Martin BJ; Golen KLV A comparison of cholesterol uptake and storage in inflammatory and noninflammatory breast cancer cells. *Int. J. Breast Cancer* 2012, 2012, 1–10.
- [48]. Tang Y; Zeng X; Liang J Surface plasmon resonance: An introduction to a surface spectroscopy technique. *J Chem Educ.* 2010, 87, 742–746. [PubMed: 21359107]
- [49]. Riss TL; Moravec RA; Niles AL; Duellman S; Benink HA; Worzella TJ; Minor Cell Viability Assays. In: Weidner J, editor. *Assay Guidance Manual*. Eli Lilly & Company and the National Center for Advancing Translational Sciences; Bethesda, MD, USA: 2004. [(accessed on December 1, 2019)]. Available online: <https://www.ncbi.nlm.nih.gov/books/NBK144065/>
- [50]. Siddique AB; Ayoub NM; Tajmim A; Meyer SA; Hill RA; Sayed KAE (–)-Oleocanthal prevents breast cancer locoregional recurrence after primary tumor surgical excision and neoadjuvant targeted therapy in orthotopic nude mouse models. *Cancers* 2019, 11, 637.
- [51]. Dutta S; Sengupta P Men and mice: Relating their ages. *Life Sci.* 2016, 152, 244–248. [PubMed: 26596563]
- [52]. Retsky M; Demicheli R; Hrushesky W; Baum M; Gukas I Surgery triggers outgrowth of latent distant disease in breast cancer: An inconvenient truth? *Cancers* 2010, 2, 305–337. [PubMed: 24281072]
- [53]. Keating GM Evolocumab: A review in hyperlipidemia. *Am. J. Cardiovasc. Drugs* 2015, 16, 67–78.
- [54]. Chatterjee P; Franklin MR Human cytochrome P450 inhibition and metabolic-intermediate complex formation by goldenseal extract and its methylenedioxyphenyl components. *Drug Metab. Dispos* 2003, 31, 1391–1397. [PubMed: 14570772]
- [55]. Hermann R; Richter OV Clinical evidence of herbal drugs as perpetrators of pharmacokinetic drug interactions. *Planta Med.* 2012, 78, 1458–1477. [PubMed: 22855269]
- [56]. He S; Nelson ER 27-Hydroxycholesterol, an endogenous selective estrogen receptor modulator. *Maturitas* 2017, 104, 29–35. [PubMed: 28923174]
- [57]. Dusell CD; Umetani M; Shaul PW; Mangelsdorf DJ; McDonnell DP 27-Hydroxycholesterol is an endogenous selective estrogen receptor modulator. *Mol. Endocrinol* 2008, 22, 65–77. [PubMed: 17872378]
- [58]. Buonaguro FM; Pauza CD; Tornesello ML; Hainaut P; Franco R; Tommasino M Cancer diagnostic and predictive biomarkers 2016. *Biomed. Res. Int* 2017, 2017, 1–2.

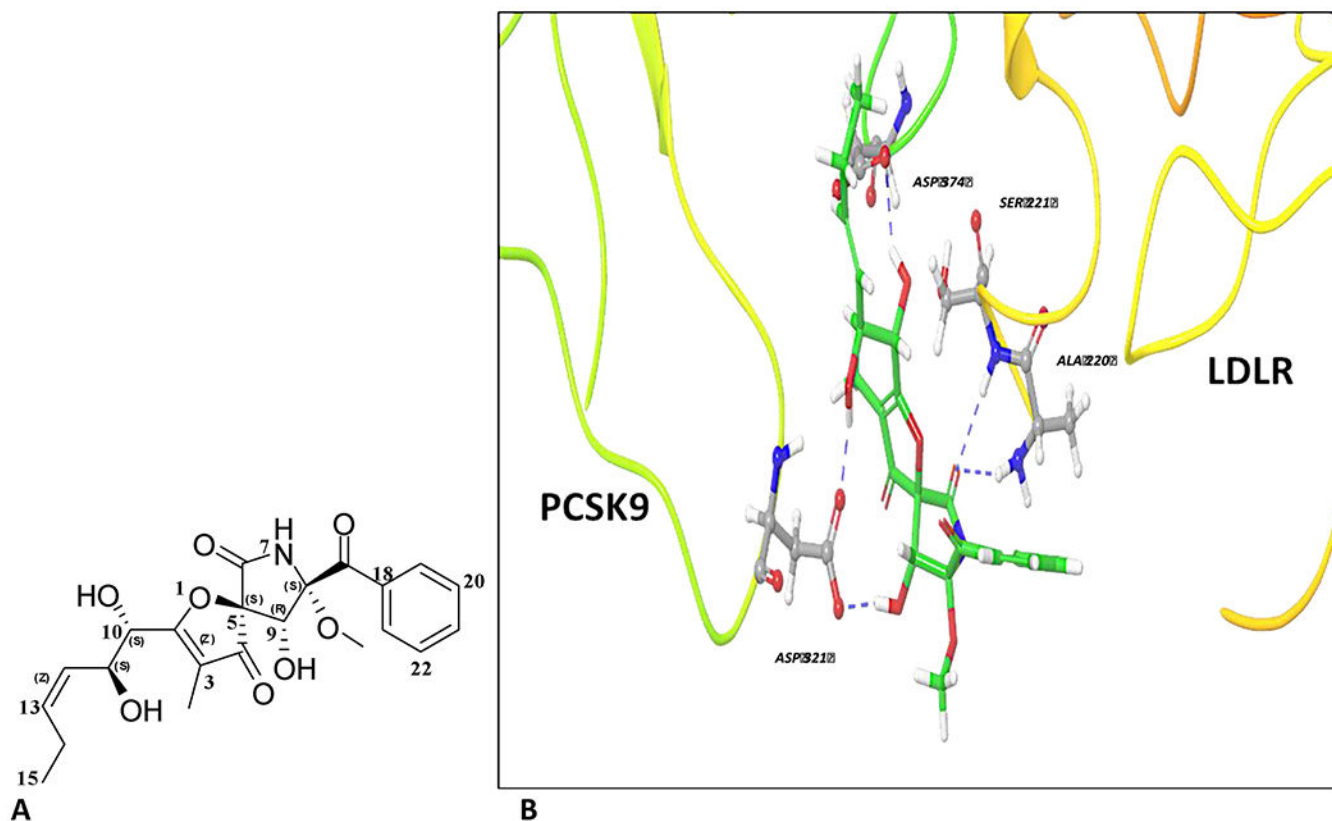
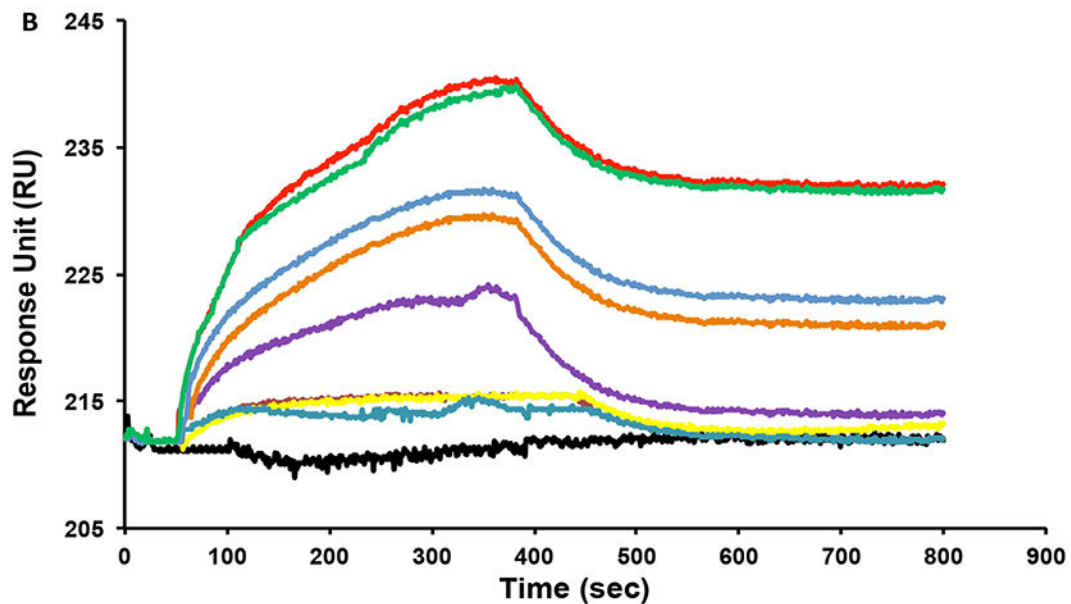
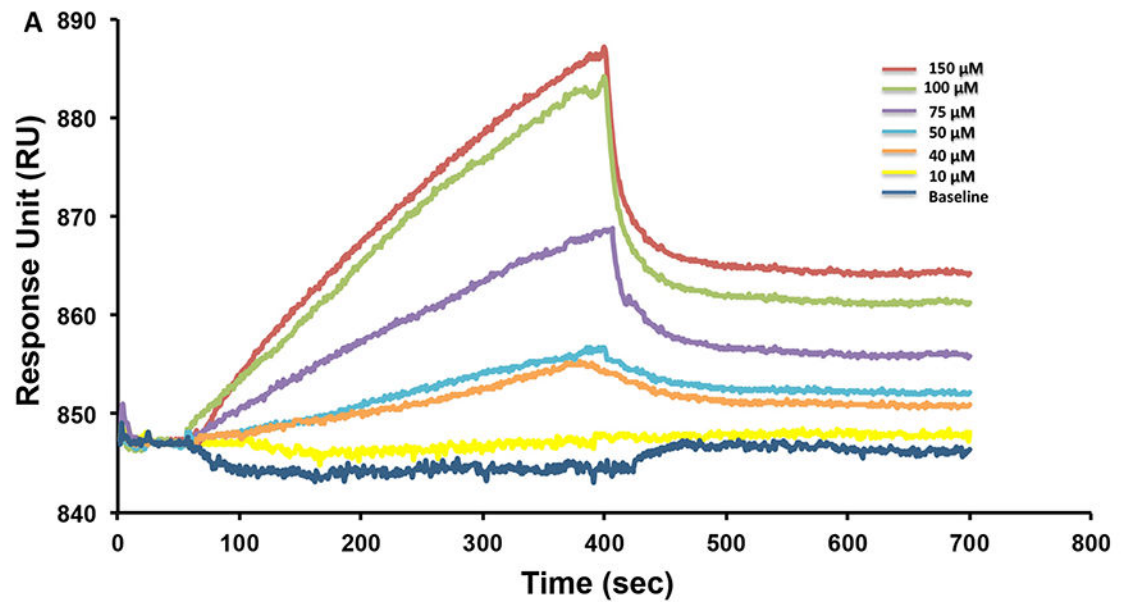


Figure 1.

Chemistry and binding mode of pseurotin A at the wild-type PCSK9 crystal structure 3GCX. **(A)** The chemical structure of pseurotin A (PS). **(B)** *In silico* binding mode of PS at the PCSK9-LDLR binding interface of PDB crystal structure 3GCX showing its important hydrogen bond (HB) interactions with the crucial ASP374 of the PCSK9 catalytic domain. The protein is shown in 3D cartoon representation. HB interactions are shown in blue dashed lines between the OH's of PS side chain along with its azaspiro carbonyl group and different amino acids in PCSK9 catalytic domain. PS's aromatic ring did not have direct binding or π - π stacking role, but it promoted proper alignment of the binding pharmacophores at PCSK9 interface in crystal structures.



— PCSK9 200 nM — Berberine 100 μ M — Pseurotin A 10 μ M — Pseurotin A 20 μ M — Pseurotin A 50 μ M
 — Pseurotin A 75 μ M — Pseurotin A 100 μ M — Pseurotin A 200 μ M — Baseline

Figure 2.

Surface plasmon resonance (SPR) validation of the PS inhibitory effects for the PCSK9-LDLR interaction. (A) SPR sensogram of PS different concentrations (150 μ M, 100 μ M, 75 μ M, 50 μ M, 40 μ M, and 10 μ M) binding to the immobilized PCSK9 in dose dependent manner. (B) SPR sensogram for competitive assay binding of PS and PCSK9 with immobilized LDLR at injection of PS with different doses (200 μ M, 100 μ M, 75 μ M, 50 μ M, 20 μ M, and 10 μ M) in the presence of 200 nM PCSK9. Berberine 100 μ M used as a negative control.

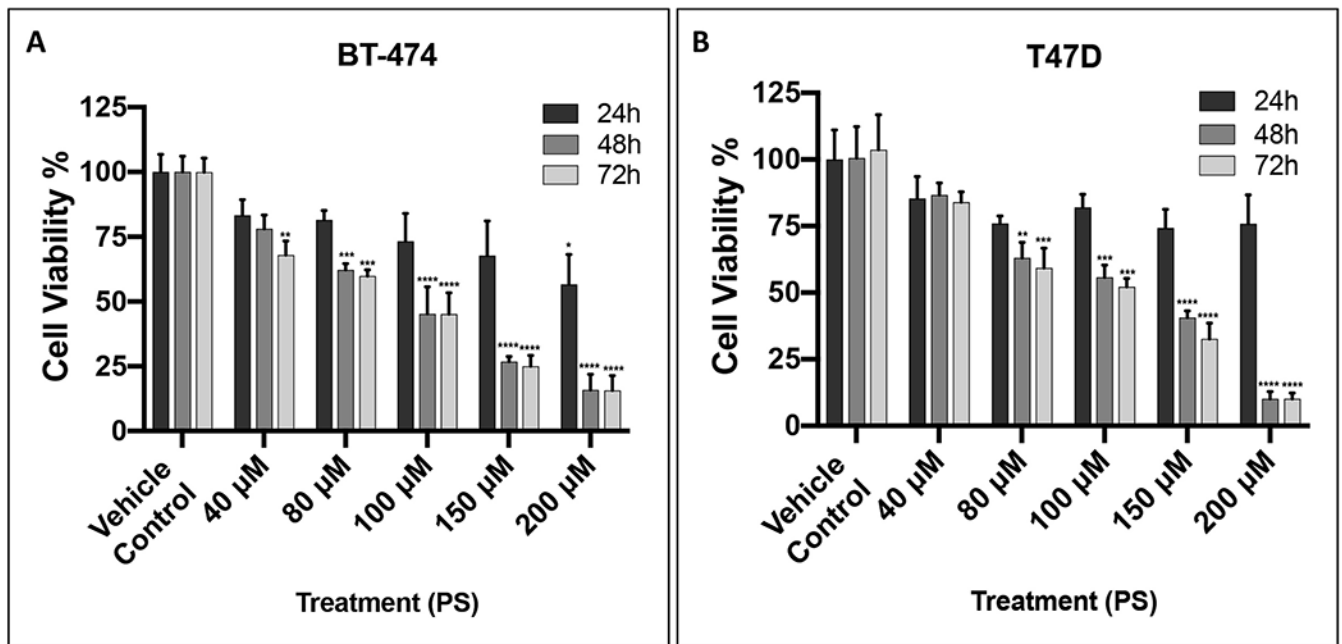


Figure 3.

Effect of different PS treatments on the growth of hormone-dependent BC cells using MTT assay. **(A)** The effect of PS treatments on the growth of BT-474 cells over 24 h, 48 h, and 72 h culture period. **(B)** The effect of PS treatments on the growth of T47D cells after 24 h, 48 h, and 72 h culture period. Cells were treated with vehicle-control or increasing concentrations of PS treatment. Results showed time and dose-dependent inhibition of BC cells viability. Vertical bars indicate mean cell count \pm SEM ($n = 6$) in each treatment group for same culture period time (* $p < 0.05$, ** $p < 0.01$, *** $p < 0.001$, and **** $p < 0.0001$ for statistical significance compared to vehicle-treated controls).

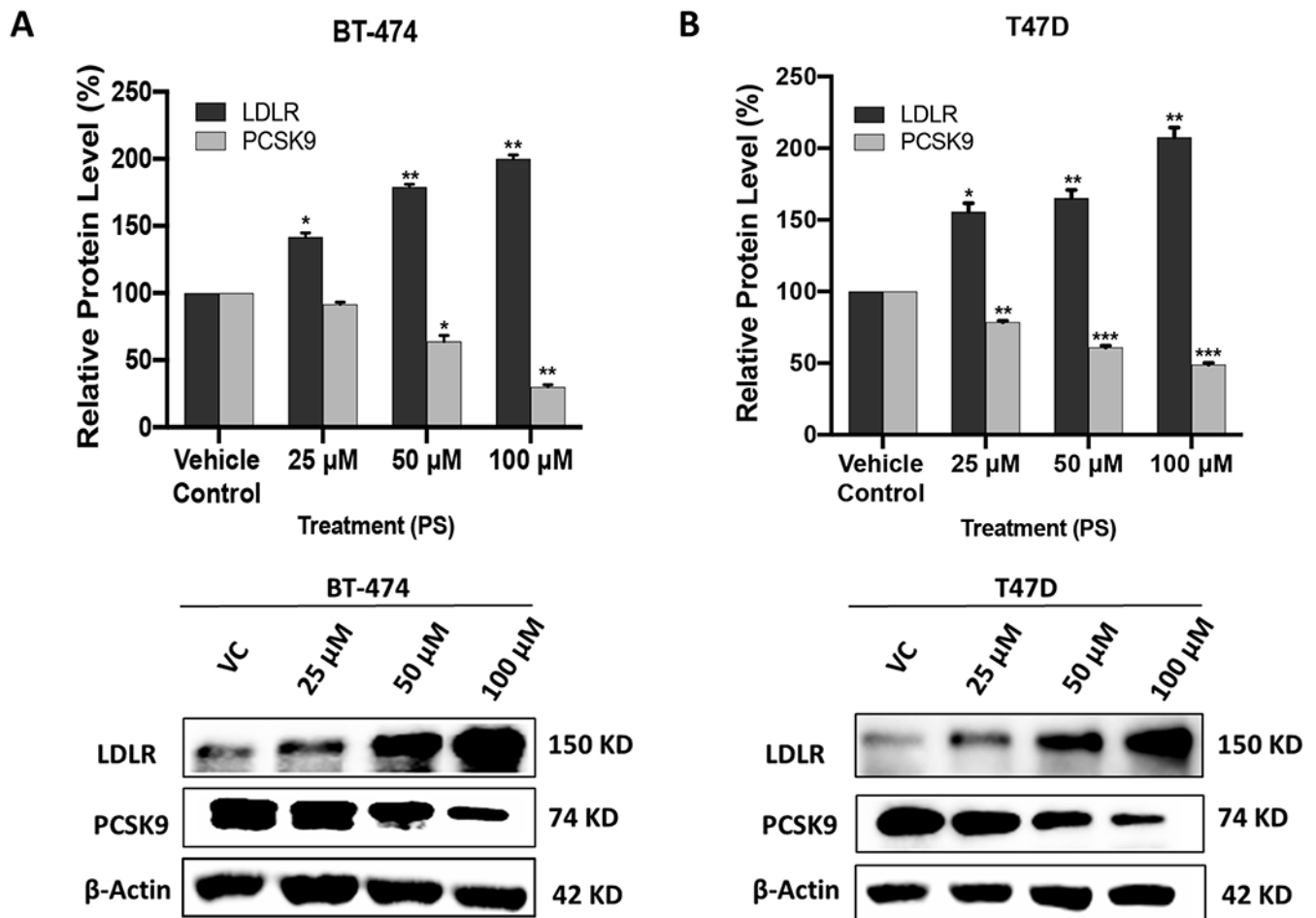


Figure 4.

Effects of PS treatments on the expression levels of PCSK9 and LDLR in BT-474 and T47D BC cell lines. Top panels represent the densitometric analysis of all blots. Bottom panels include representative Western blots for LDLR and PCSK9. (A) Expression of LDLR and PCSK9 in BT-474 cells treated with vehicle control, 25 μ M, 50 μ M, and 100 μ M PS over 72 h. (B) Expression of LDLR and PCSK9 in T47D cells treated with vehicle control, 25 μ M, 50 μ M, and 100 μ M PS over 72 h. Scanning densitometry was obtained for all blots, carried out in triplicate, and the integrated optical density of each band was normalized with the corresponding density found for β -actin in the same blot. Results shown in the bar graphs under their respective Western blot images. Vertical bars in the graph indicate the normalized integrated optical density of bands visualized in each lane. * $p < 0.05$, ** $p < 0.01$, and *** $p < 0.001$, compared to their respective vehicle-treated control group.

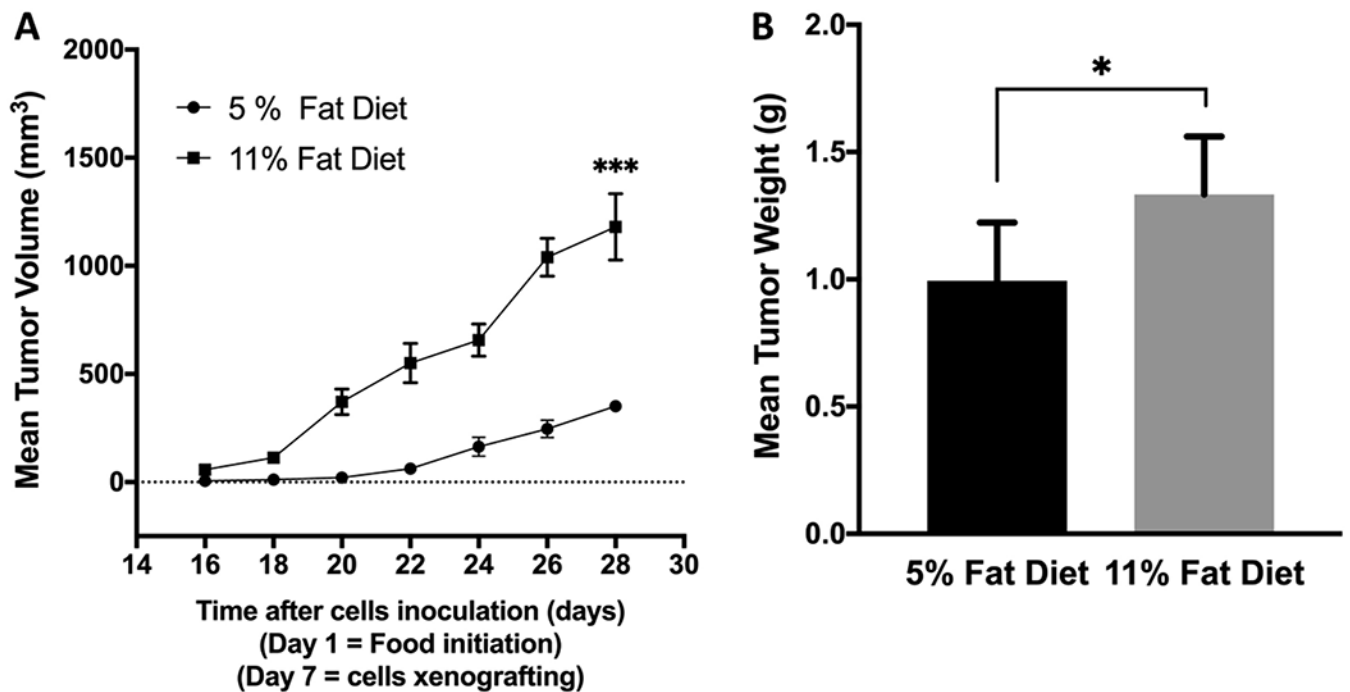


Figure 5.

Comparison of the effects of the intake of high fat diet (11% fat) versus regular chow diet (5% fat) on the progression of the hormone-dependent BC BT-474 cells in orthotopic nude mouse xenograft model. **(A)** Comparison of the mean BT-474 cell tumors volume. Points represent the mean tumor volumes for each experimental group. **(B)** Comparison of the mean BT-474 cell tumors weight. Error bars indicate SEM for each experimental group. * $p < 0.05$ and *** $p < 0.001$ for statistical significance compared to normal chow diet fed group.

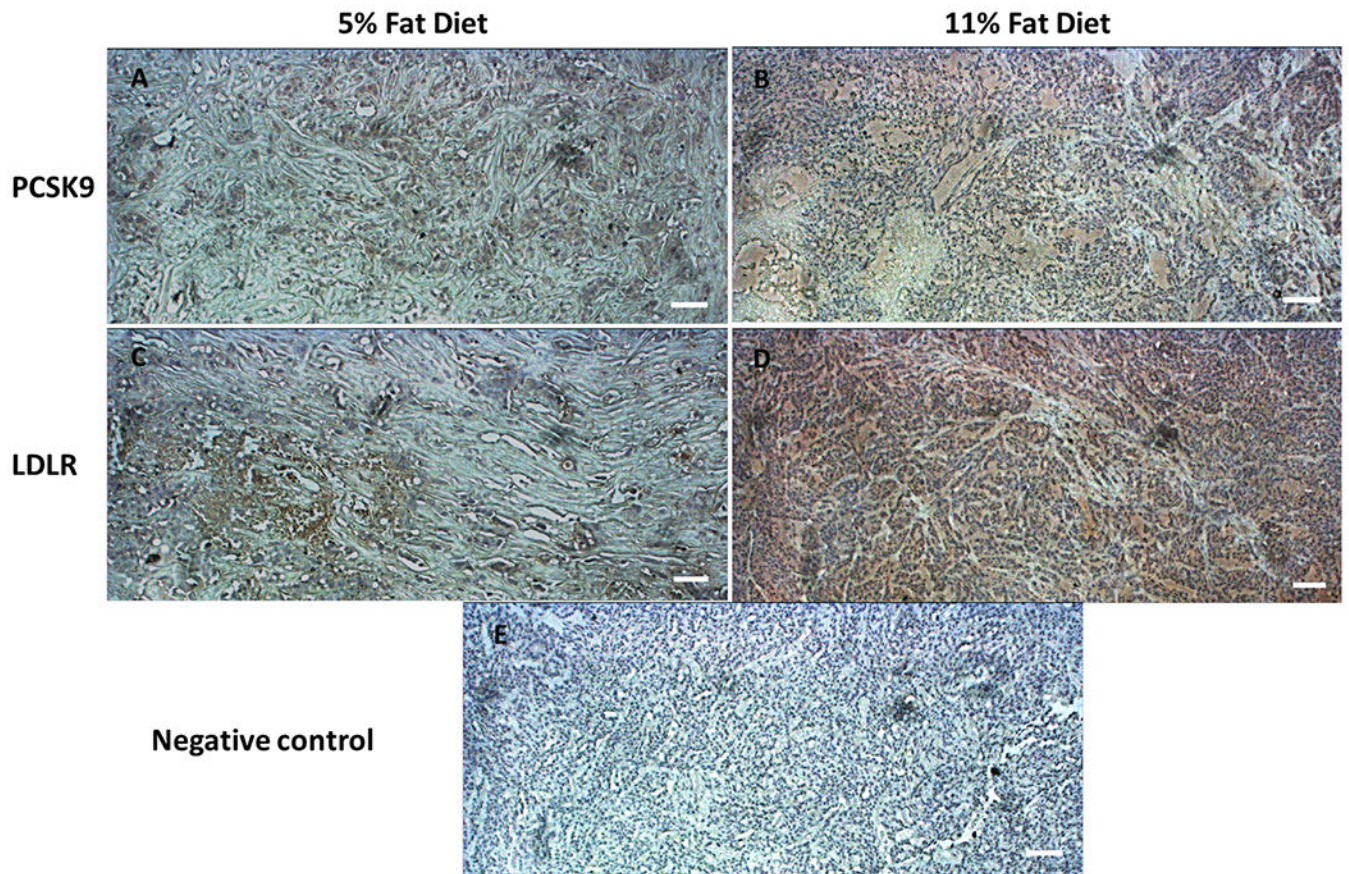


Figure 6.

Immunohistochemical comparison of the effects of the intake of HFD (11% fat) versus regular chow diet (5% fat) on the expression of PCSK9 and LDLR proteins in the hormone-dependent breast tumors. IHC visualization of the expression of PCSK9 in BT-474 breast tumor tissues collected from mice fed on regular chow diet (A) and HFD (B). IHC visualization of the expression of LDLR in BT-474 breast tumor tissues collected from regular chow diet (C) and HFD (D) fed mice. (E) Negative control stained BT-474 breast tumor tissue without antibodies. Data show high differentiated and expression levels of PCSK9 and LDLR (brown color) in breast tumor tissues collected from HFD fed mice versus regular chow diet fed mice. Magnification 10X. Scale bars represent 100 μm.

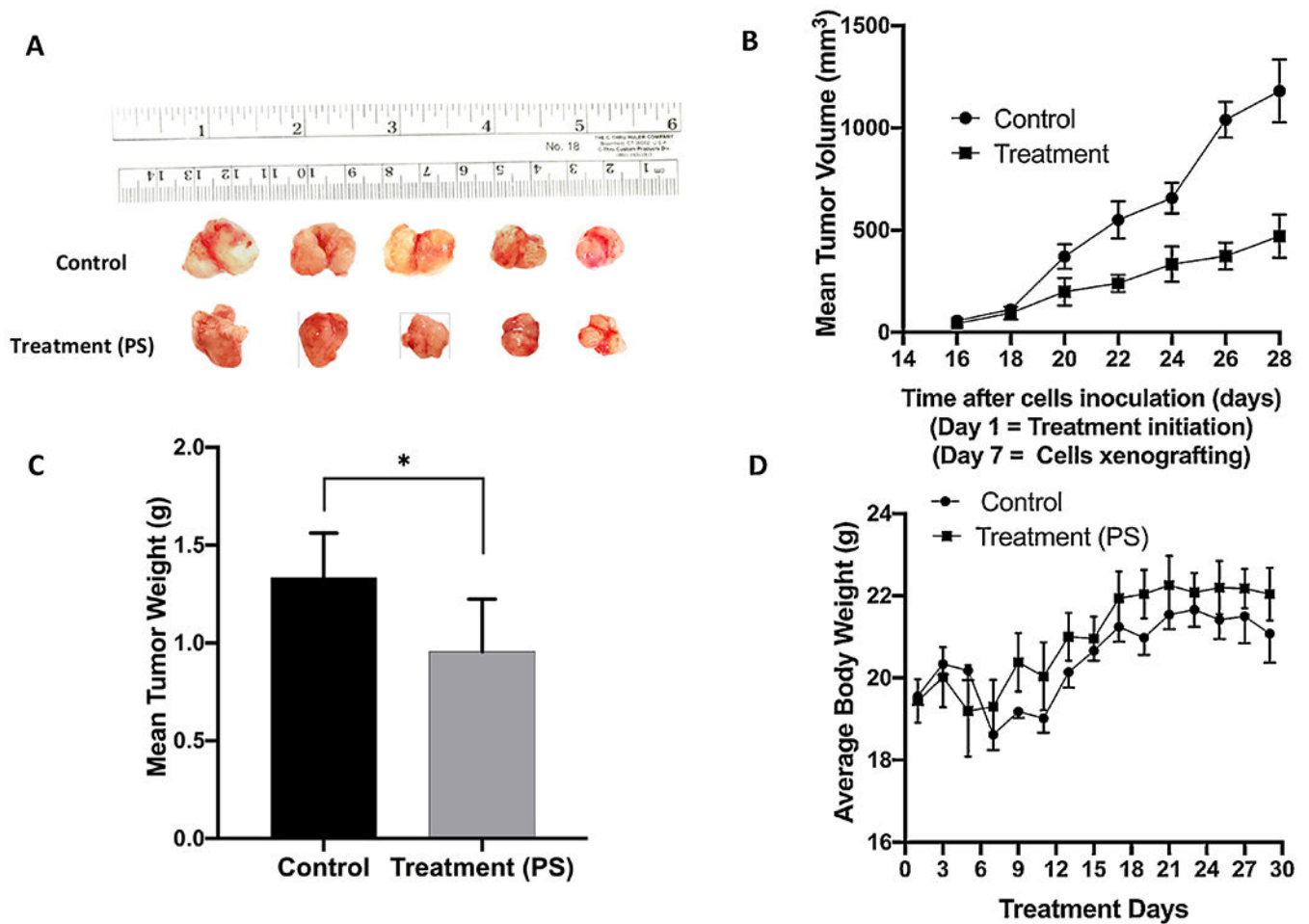


Figure 7.

Effects of oral PS treatment on the progression of the orthotopically xenografted BC cells BT-474 in HFD-fed athymic nude mice. (A) Representative primary tumors of each experimental group collected after surgical excision surgeries. Top row is the vehicle-treated control group, and the bottom row is the PS-treated group, 10 mg/kg, oral, 7X/week. (B) Comparative monitoring of the mean BT-474 cells tumor volume for the PS-treated daily oral 10 mg/kg mice versus the vehicle-treated control group over the experiment duration. Points represent the mean tumor volumes, and error bars represent the SEM for each experimental group. (C) The mean tumor weights in PS-treated versus vehicle control-treated at the experiment end. Error bars indicate SEM. * $p < 0.05$ for statistical significance compared to vehicle-treated control group. (D) Mice body weight-monitoring over the experiment course. Points represent the mean body weight for animals in each group. Error bars indicate SEM.

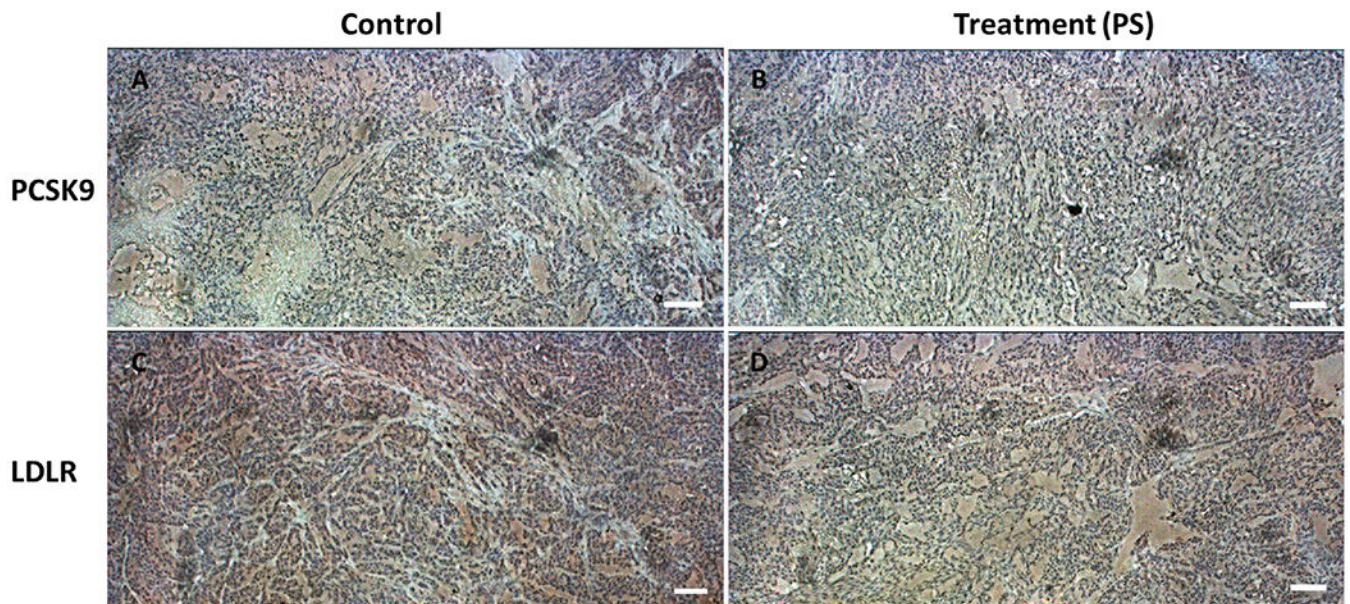
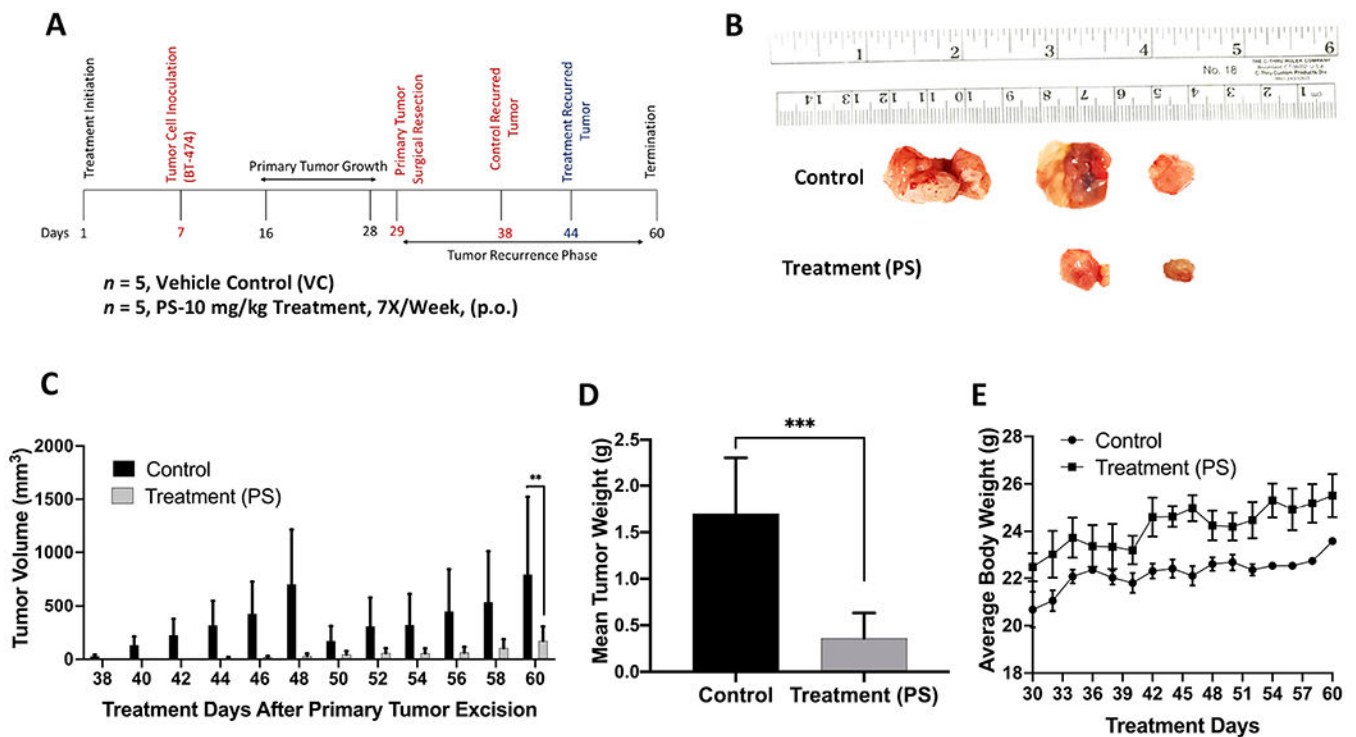


Figure 8.

Immunohistochemical comparison of the effect of PS versus vehicle control treatments on the expression of PCSK9 and LDLR proteins in orthotopically xenografted BT-474 breast tumor cells in athymic nude mouse model. IHC visualization of the expression of PCSK9 in BT-474 breast tumor tissues collected from mice treated with vehicle control (**A**) and 10 mg/kg daily oral PS (**B**). (**C**) IHC visualization of the expression of LDLR in BT-474 breast tumor tissues collected from mice treated with vehicle control (**C**) and 10 mg/kg daily oral PS (**D**). Data show high differentiated and expression level of PCSK9 (brown color) in vehicle control tissue versus low expression level in PS-treated tissues. The IHC visualization of LDLR showed comparable expression pattern in both groups. Magnification 10X. Scale bars represent 100 μm .

**Figure 9.**

Recurrence suppressive effects of oral PS treatment after BT-474 BC cells orthotopically xenografted in athymic nude mice, allowed to grow tumors, followed by primary tumor surgical excision. (A) Overview of the experimental design. (B) Collected recurred tumors of each experimental group after the experiment completion. The top row shows the vehicle-treated control group recurred tumors (3 out of 5), while the bottom row shows tumors collected from PS-treated mice, 10 mg/kg, oral, 7X/week (2 out of 5). (C) Comparative monitoring of the mean recurrence tumor volumes for PS versus vehicle control-treated mice over the recurrence experiment course. Bars represent the mean tumor volume; error bars represent the SEM for each experimental group. ** $p < 0.01$ for statistical significance comparing to vehicle-treated control group. (D) Comparison of the mean recurred tumors weights for PS-treated versus vehicle control-treated mice at the experiment end. Error bars indicate SEM. *** $p < 0.001$ for statistical significance. (E) Mice body weight-monitoring data over the experiment course. Points represent the mean body weights for animals in each group. Error bars indicate SEM.

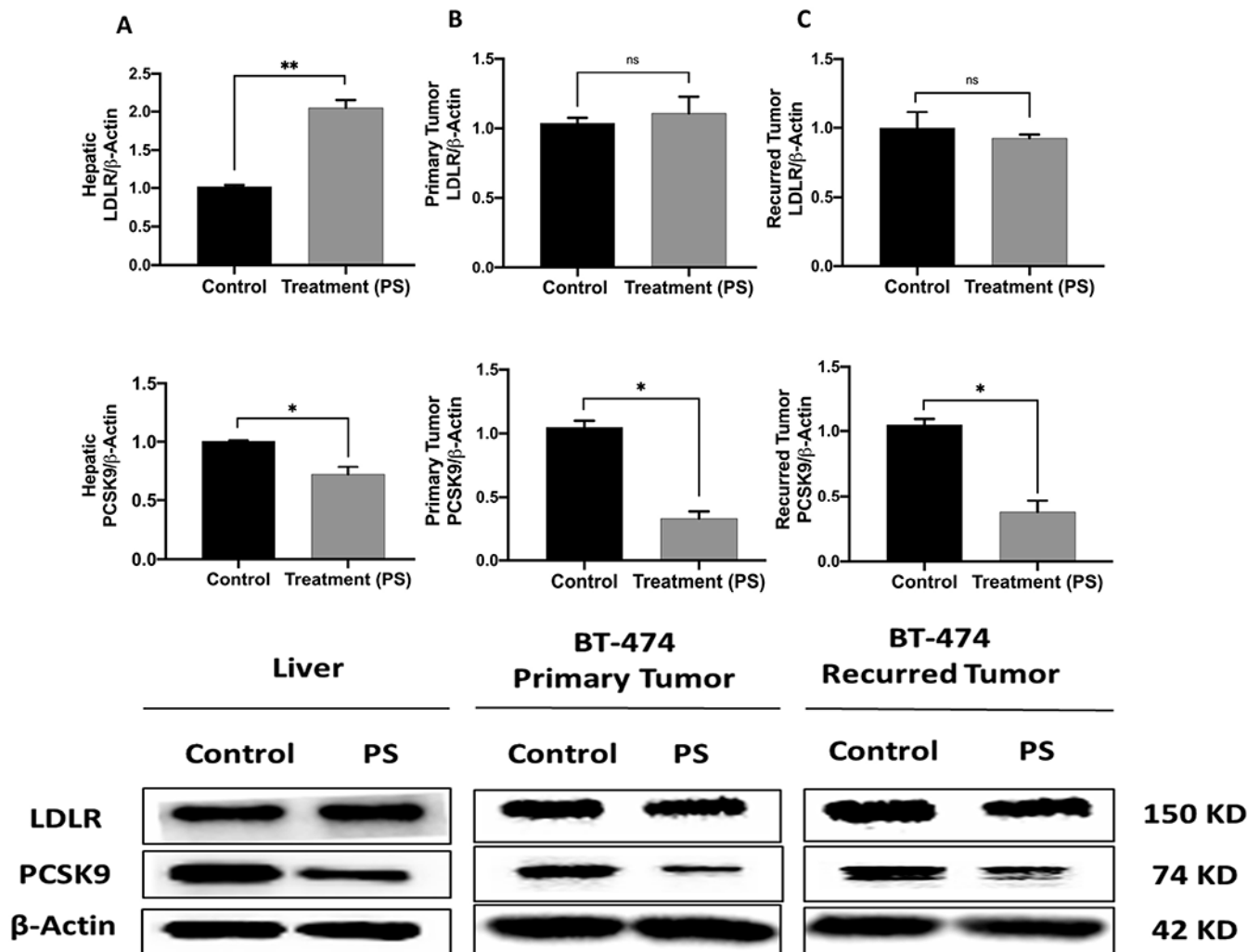


Figure 10.

The *in vivo* effects of PS treatments on the PCSK9 and LDLR expression levels in orthotopically xenografted BT-474 BC cells in athymic nude mice and in collected animal livers. Top panels represent the densitometric analysis of all blots and bottom panels are representative Western blots for LDLR and PCSK9. (A) The expression of levels of LDLR and PCSK9 in nude mice liver samples collected after the experiment end. (B) The expression levels of LDLR and PCSK9 in breast primary tumors surgically resected from BT-474 cells growth model animals. (C) The expression levels of LDLR and PCSK9 in BT-474 cells recurrence tumors collected after the experiment end. Scanning densitometry was obtained for all blots, carried out in triplicate, and the integrated optical density of each band was normalized with the corresponding density found for β -actin in the same blot, results shown in the bar graphs under their respective western blot images. Vertical bars in the graph indicate the normalized integrated optical density of bands visualized in each lane. * $p < 0.05$ and ** $p < 0.01$ for statistical significance compared to respective vehicle-treated control group.

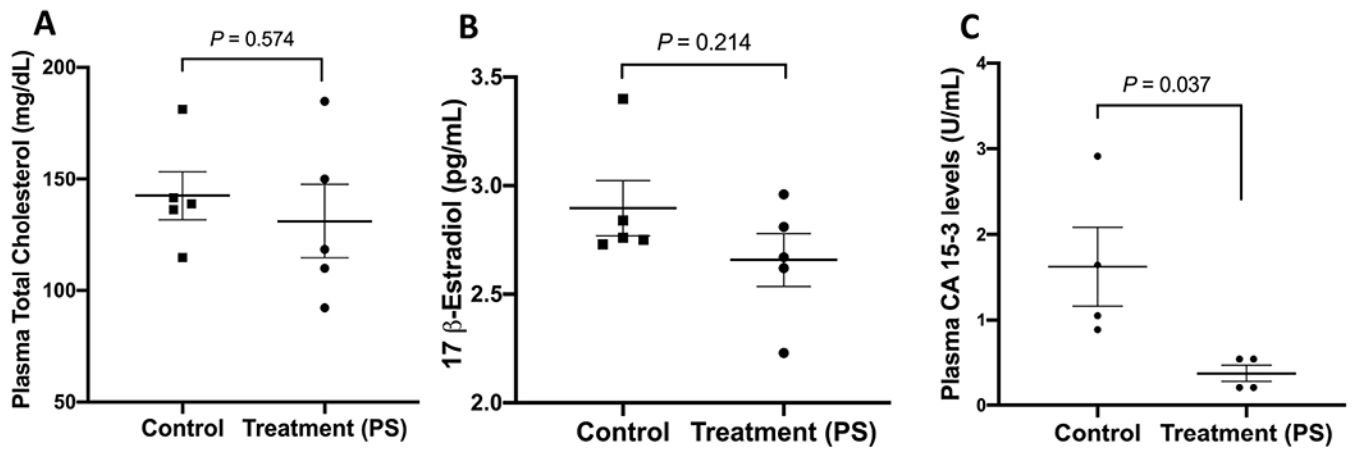


Figure 11.

Effects of PS treatments on the plasma total cholesterol, 17β-estradiol, and CA 15-3 levels in BT-474 tumors in HFD fed nude mice. (A) Comparison of the mean plasma total cholesterol levels of PS-treated versus vehicle control-treated in BT-474 tumors at the experiment end. (B) Comparison of the 17β-estradiol plasma levels of PS versus vehicle control-treated nude mice xenografted BT-474 tumor cells at the experiment end. (C) Comparison of the BC recurrence marker CA 15-3 plasma levels of PS versus vehicle control-treated nude mice xenografted BT-474 tumor cells at the experiment end. $p > 0.05$ is statistically not significant.

Table 1.

Comparison of the PS viability inhibitory effects (IC₅₀) against the hormone-dependent BC cell lines.

PS	24 h	48 h	72 h
BT-474 (IC₅₀)	260.83 μ M	98.88 μ M	93.64 μ M
T47D (IC₅₀)	267.48 μ M	120.92 μ M	113.08 μ M

Author Manuscript

Author Manuscript

Author Manuscript

Author Manuscript